Astronomy & Astrophysics manuscript no.
(will be inserted by hand later)

Dynamical Friction in Inhomogeneous Systems

Andreas Just and Jorge Peñarrubia

Astronomisches Rechen-Institut, Mönchhofstraße 12-14, 69120 Heidelberg, Germany

Received / Accepted

Abstract. Dynamical friction plays an important role in the orbital evolution of massive objects in a sea of lighter particles (satellite galaxies in Dark Matter haloes, Super-massive Black Holes in galaxy centres, massive stars in star clusters). The standard formula of Chandrasekhar based locally on an isotropic and homogeneous distribution function worked in the past surprisingly well. But in the last years, due to the improved numerical facilities, systematic deviations were observed. In recent work, three aspects of improvements are discussed: Variation of the Coulomb logarithm with position along the orbit, anisotropic velocity distribution functions, and the effect of the local density gradient. In this paper we discuss the effect of a position dependent Coulomb logarithm and the influence of the local density gradient on the dynamical friction force. We apply the new formulae to the orbital evolution of satellite galaxies in the Dark Matter halo. We compare semi-analytical computations with numerical N-body calculations for the analysis of the different approaches to the dynamical friction formula. We find that for a maximum impact parameter proportional to the local scale length, there is a significant improvement of the orbital fit and reduction of the circularisation of the orbit as is observed in most numerical calculations. The additional force due to the density gradient contributes up to 10% to the total friction force, but shows a completely different behaviour. The net effect on the orbital evolution is very small in the first tests. We expect a significant effect on the circularisation and precession rate of the orbits for more eccentric orbits and larger masses of the massive object relative to the enclosed background mass.

Key words. dynamical friction – Galaxies: kinematics and dynamics – Galaxies: interactions – dark matter

1. Introduction

Since N-body calculations including many gravitating particles are extremely time-consuming even with the fastest available computers, there are many applications where an analytical approximation of the net effect of the mutual gravitational interaction as a correction to the mean field force is very helpful. The basic effect on massive particles like satellite galaxies in the Dark Matter halo of the parent galaxy or massive stars in a stellar system is dynamical friction due to the gravitational wake induced by gravitational focusing of the particles of the ambient medium. In the past decades the standard friction formula of Chandrasekhar (Chandrasekhar 1943, Binney & Tremaine 1987, hereafter B-T, Eq. (7-17)) given by

$$\dot{\boldsymbol{v}}_{\mathbf{hom}} = -C_{\mathrm{Ch}} G_{\mathrm{hom}}(X) \boldsymbol{e}_{\mathbf{v_M}} \quad \text{with} \tag{1}$$

$$G_{\mathrm{hom}}(X) = \frac{\langle \ln \Lambda \rangle}{X^2} \left[erf(X) - \frac{2X}{\sqrt{\pi}} \exp(-X^2) \right]$$

$$C_{\mathrm{Ch}} = \frac{2\pi G^2 mn(M+m)}{\sigma^2} \quad \text{and} \quad X = \frac{|v_{\mathrm{M}}|}{\sqrt{2}\sigma} \tag{2}$$

worked surprisingly well. Here M and v_{M} are the mass and velocity of the massive body; m, n, σ are mass, number density, and velocity dispersion of the particles of the ambient medium, respectively. $\langle \ln \Lambda \rangle$ is the Coloumb logarithm measuring the effective range of relevant impact parameters. Usually one fixed value of the Coulomb logarithm is used for the friction along the whole orbit or even for all orbits in the system. For consistency with the improved description of a position dependent Coulomb logarithm $\ln \Lambda$ in this paper we used here (informal) averaging brackets. The index 'hom' is introduced to make clear that the standard force arises from the locally homogeneous density distribution of the ambient medium. The force arising from the local density gradient will be labelled by 'inh'. For details see below.

Originally the term 'dynamical friction' comes from the Fokker Planck approximation of relaxation processes in collisionless matter. Dynamical friction appears together with the diffusion process in velocity space due to 2-body correlations. Dynamical friction is first order in the velocity change Δv and diffusion is second order in Δv. Diffusion increases statistically the energy of the particles and dynamical friction decreases the particle energy as a competing process to allow for a Maxwellian distribution in equilibrium. In the meanwhile dynamical friction was generalised to collisional matter using different methods: for stars in the ISM with a quasi linear perturbation theory (Just et al. 1986), for objects in a homogeneous gas using time-dependent linear perturbation theory (Just & Kegel 1990, Ostriker 1999) or numerical calculations (Sánchez-Salcedo & Brandenburg 1999). For an applica-

Send offprint requests to: A. Just
Correspondence to: just@ari.uni-heidelberg.de

tion to satellite galaxies moving in a gaseous spherical halo see Sánchez-Salcedo & Brandenburg (2001).

In astrophysics basically two different kinds of applying dynamical friction turned out to be important. The first one is the effect of dynamical friction on the evolution of subpopulations of more massive particles: dynamical cooling and mass segregation. This is important in the evolution of globular clusters when using a mass spectrum for the stars or when taking into account the different masses of main sequence stars and stellar remnants. For galaxies in clusters of galaxies and for stars in young star clusters mass segregation may also be relevant. The time scale for mass segregation is essentially the relaxation time of the system corrected by some function of the individual masses of the bodies. In order to point out the difference again: dynamical heating (of galactic disks due to massive Dark Matter objects, satellite galaxies or giant molecular clouds e.g.) is an effect of the diffusion process in the component of light particles describing the energy gain, which corresponds to the energy loss of the massive particles due to dynamical friction. In general, the evolution of a dynamically hot component (usually that with more massive particles) is dominated by dynamical friction and the evolution of a dynamically cool component is determined by the diffusion process.

The second type of application concerns the dynamics of individual massive objects like satellite galaxies in the Dark Matter halo or super massive black holes (SMBHs) in the central star cluster of the hosting galaxy. Due to the high mass ratio M/m of the individual masses, the kinetic energy of the massive body is much higher than the energy of the particles of the ambient medium. Therefore the effect of diffusion on the massive body, which results in some random walk, can be neglected. The main effect of the dynamical friction force is a deceleration of the satellite (from here on we discuss dynamical friction for satellite galaxies moving in the Dark Matter halo of the parent galaxy, but similar arguments and results hold for other applications, too) leading to an energy loss and decay of the orbit. But the term 'friction' is somewhat misleading, because the effect of dynamical friction depends on the symmetries of the distribution function of the Dark Matter particles. Instead of braking the satellite, there can be also a bending or even an acceleration of the satellite (as we will show below). In any case the orbit average yields a net deceleration of the satellite, of course.

In this paper we want to investigate the effect of the local density gradient of the ambient medium on dynamical friction. Since the assumption of a locally homogeneous distribution of collision partners is one of the very basic foundations of the dynamical friction formula, it is worthwhile to discuss here again the physical frame in which the standard Chandrasekhar dynamical friction formula is derived. The satellite has mass M, velocity $\boldsymbol{v}_{\mathrm{M}}$, and position $\boldsymbol{r}_{\mathrm{M}}$. The Dark Matter particles with mass m are described by the distribution function $f(\boldsymbol{r},\boldsymbol{v})$ and the relative velocity of the collision partners is given by $\boldsymbol{V_0}=\boldsymbol{v}-\boldsymbol{v}_{\mathrm{M}}$. There are basically two types of assumption going into Eq. 1, the fundamental physical approximations to get the net acceleration as a superposition of isolated 2-body encounters on one hand side, and technical simplifications to get finally a simple analytical expression on the other hand side. The fundamental assumptions are:

Perturbation approximation: The acceleration is computed relative to the unperturbed motion and the effect of all encounters are added by the superposition principle. The offset in phase space due to the (many!) other encounters at the same time is neglected. Therefore the deflection of the satellite due to one encounter must be small. the restriction for the Dark Matter particles are weaker, because here the overall change of the distribution function must be small. That means, that relatively few large angle encounters can consistently be taken into account, although the jumps in velocity space for these Dark Matter particle is large.

Straight-line approximation: The unperturbed motion of both particles has a constant velocity. Acceleration of the 2 bodies due to the mean field are neglected. A constant mean field force would lead to an additional shift in phase space during the encounter, but to the same deflection. Taking tidal fields into account would give corrections to the relative accelerations. In order to include the effects of the mean field a new definition of the local rest frame is necessary to handle the changing unperturbed relative velocity vector $\boldsymbol{V_0}$.

Local approximation in space and time: The parameters of the full encounter are determined by the local distribution function, i.e. the impact parameter $\boldsymbol{b}$ (a vector in the plane perpendicular to $\boldsymbol{V_0}$) and the unperturbed relative velocity $\boldsymbol{V_0}$ is given by the relative position and velocity at $t=-\infty$. Additionally the rate of encounters with given $\boldsymbol{V_0}$ and $\boldsymbol{b}$ is also determined by the local distribution function $f(r,v)|_{r_{\mathrm{M}}}$. Here the changing offset of the Dark Matter particle in phase space during the collision is neglected. This approximation has two steps. The first, which is basic, is to adopt the distribution function at minimum distance of the unperturbed motion given by the impact parameter. The second step is a technical approximation of the spatial dependence on $\boldsymbol{b}$ (see below).

These basic assumptions cannot be relaxed easily. Based on these assumptions, the effect of the grainy structure of the background matter can be computed in lowest order using the deflection $(\Delta v_{\mathrm{M}\|}, \Delta v_{\mathrm{M}\perp})$ due to isolated 2-body encounters with

$$\begin{aligned} \boldsymbol{\Delta v}_{\mathrm{M}\|} &= \frac{2m\boldsymbol{V_0}}{(M+m)}\left[1+\frac{b^2V_0^4}{G^2(M+m)^2}\right]^{-1} \\ &= \frac{2Gm}{a(V_0)}\frac{\boldsymbol{V_0}}{V_0^2}\left[1+\frac{b^2}{a(V_0)^2}\right]^{-1} \qquad (3) \end{aligned}$$

$$\begin{aligned} \boldsymbol{\Delta v}_{\mathrm{M}\perp} &= \frac{2m\boldsymbol{b}V_0^3}{G(M+m)^2}\left[1+\frac{b^2V_0^4}{G^2(M+m)^2}\right]^{-1} \\ &= \frac{2Gm\boldsymbol{b}}{a(V_0)^2V_0}\left[1+\frac{b^2}{a(V_0)^2}\right]^{-1} \qquad (4) \end{aligned}$$

$$\text{with} \qquad a(V_0)=\frac{G(M+m)}{V_0^2} \qquad (5)$$

(B-T, Eqs. (7-10a,b)) for a given impact parameter $\boldsymbol{b}$ and relative velocity $\boldsymbol{V_0}$. Here $a(V_0)$ is the impact parameter for a 90 degree deflection. From this acceleration we have to substract the acceleration along the unperturbed orbit. Taking the difference is necessary in a self-gravitating system, since otherwise we would count the effect of the local mean field twice. For the net effect of 2-body encounters one has to sum over all collision partners. In order to get analytic results, further computational simplifications and additional approximations are usually made.

Local homogeneous distribution function: By assuming a homogeneous density distribution for the collision partners, the integration over the directions of the impact parameters $\boldsymbol{b}$ leads to a vanishing contribution of the velocity change perpendicular to the relative velocity $\boldsymbol{\Delta v}_{\mathrm{M}\perp}$. This term corresponds to the 0. order Taylor expansion of the local density. We will include the 1. order term in order to investigate the effect of a local density gradient.

Isotropic Gaussian distribution function: With an isotropic velocity distribution function, the friction term arising from $\boldsymbol{\Delta v}_{\mathrm{M}||}$ is antiparallel to the motion of the satellite $\boldsymbol{v}_{\mathrm{M}}$. Then dynamical friction works like a real drag force decelerating the satellite galaxy. The Gaussian shape is the best we know from collisionless Dark Matter particles. There is no reason to assume large deviations leading to very different results.

Constant Coulomb logarithm: The slow dependence on the relative velocity V_0 of the Coulomb logarithm is neglected and substituted implicitly by an appropriate mean value for the integration over V_0. For the homogeneous friction term this is a robust approximation, but for the inhomogeneous term a singularity for small V_0 would occur.

There are some attempts in the literature generalising Chandrasekhars formula, but none of them is commonly used. Binney (1977) started with analytical expressions for a generalisation in two aspects. For an anisotropic Gaussian he showed that the dynamical friction force is no longer parallel to the satellite velocity and leads to a decreasing inclination of the orbit in a flattened Dark Matter halo (DMH). A systematic analysis of dynamical friction in anisotropic, flattened DMHs will be presented in Peñarrubia et al. (2003). In a recent work Tsuchiya & Shimada (2000) investigated the effect of an anisotropy on the circularisation of orbits in spherical systems. Binney (1977) also discussed the effect of a local density gradient in the same way as we will do here. He computed the inhomogeneous friction term for vanishing velocity of the massive object and showed that for an application to galaxies in a cluster of galaxies, this inhomogeneous term is small compared to the (standard) homogeneous friction term and can be neglected. In a recent paper Del Popolo & Gambera (1999) give an investigation of dynamical friction in inhomogeneous distributions on a very theoretical level. In contrast to their conclusions, their results do not hold for a general inhomogeneous density distribution, because they adopted in their Eq. (12) a power law distribution spherically symmetric around the test star. Due to this symmetry, they find only a nonlinear dependence on the amount of dynamical friction. But the force remains parallel to the velocity of the test star and leads to a deceleration.

In the standard formula (Eq. 1) there are some local parameters (background density, velocity dispersion, and Coloumb logarithm), which in general depend on position of the massive particle. Often the system is implicitly assumed to be isothermal, and for the Coulomb logarithm a constant global value $\langle \ln \Lambda \rangle$ is chosen or fitted. Toomre (1976) argued for an application to the motion of the Magellanic clouds, that a maximum impact parameter proportional to the distance to the centre of the Dark Matter halo is more appropriate. This idea came up again recently in order to explain differences between numerical and semi analytical computations in the decay rate of satellite galaxies in the late phases (Hashimoto et al. 2002). A constant Coulomb logarithm overestimates dynamical friction in the inner part of the Dark Matter halo.

In this paper we investigate in detail the effect of the local density gradient on dynamical friction. We start in Sect. 2 with a detailed discussion of the collision rate for the 2-body encounters and the structure of the Coulomb logarithm with all its parameter dependences. In Sect. 3 we compute the inhomogeneous dynamical friction for an isotropic distribution function including a reanalysis of the homogeneous friction force (corresponding to the standard friction) for a consistent comparison of both parts. In Sects. 4 and 5 we apply the new formulae to a typical satellite orbit in the Dark Matter halo of the Milky Way and discuss the effect of the improved Coulomb logarithm and of the inhomogeneous friction term. Section 6 contains a discussion of the relevance of using a position dependent Coulomb logarithm and of the inhomogeneous force for other applications (super massive black holes in galactic cores) and other aspects (circularisation of the orbits).

2. Encounter rates and the Coulomb logarithm

In this section we discuss the encounter rate and perform the integration over impact parameters for the homogeneous and the inhomogeneous contribution to dynamical friction. General symmetries of the force and the properties of the Coulomb logarithm are described in detail.

2.1. Encounter rate and mean field correction

We use a local coordinate system (p, q, s) with s parallel to $\boldsymbol{V_0}$ and (p, q) the plane of impact parameters perpendicular to $\boldsymbol{V_0}$ (see Fig. 12). The integration over s is substituted by the encounter rate $n(r)|\boldsymbol{V_0}|$ with $\boldsymbol{r} = \boldsymbol{r}_{\mathrm{M}} + \boldsymbol{b}$ using formally a 3-dimensional impact parameter in vectorial form, if necessary, given by $\boldsymbol{b} = (p, q, 0) = b(\cos\phi, \sin\phi, 0)$. The rate of encounters for given relative velocity $\boldsymbol{V_0}$ and impact parameter $\boldsymbol{b}$ is then

$$\mathrm{d}\nu(\boldsymbol{b}, \boldsymbol{V_0}) = |\boldsymbol{V_0}| n(\boldsymbol{r}) f(\boldsymbol{v}) \mathrm{d}p \mathrm{d}q \mathrm{d}^3 V_0 \tag{6}$$

the Dark Matter particles are counted, when they are crossing the (p, q)-plane. The density gradient parallel to $\boldsymbol{V_0}$ corresponds to an acceleration due to mean field, because the phase space density along (unperturbed) orbits is constant in equilibrium. The effect on the timing during the encounter can be accounted for only, when tidal fields are taken into account. Acceleration due to the mean field will not be included here.

The density gradient perpendicular to $\boldsymbol{V_0}$ directly changes the encounter rate. This dominant effect of the local inhomogeneity will be included.

Since we are interested in the additional acceleration due to the grainy structure of the background distribution, we have to take the difference of the acceleration of the perturbed orbit and that of the unperturbed orbit. Particles moving at the unperturbed orbits with impact parameter $\boldsymbol{b}$ and relative velocity $\boldsymbol{V_0}$ correspond to a 'line' of constant density $mn(\boldsymbol{r})f(\boldsymbol{v})\mathrm{d}p\mathrm{d}q\mathrm{d}^3V_0$ along s, that is parallel to V_0. By symmetry, only the component parallel to $\boldsymbol{b}$ contributes and we find

$$\begin{aligned}\dot{\boldsymbol{v}}_{\mathbf{M0}} &= \int Gmn(\boldsymbol{r})f(\boldsymbol{v})\int_{-\infty}^{\infty}\frac{\boldsymbol{b}\mathrm{d}s}{\sqrt{b^2+s^2}^3}\mathrm{d}p\mathrm{d}q\mathrm{d}^3V_0 \\ &= \int\frac{2Gmn(\boldsymbol{r})\boldsymbol{b}}{b^2}f(\boldsymbol{v})\mathrm{d}p\mathrm{d}q\mathrm{d}^3V_0 \qquad (7)\end{aligned}$$

for the effect along the unperturbed motion. This acceleration must be substracted from the acceleration due to 2-body encounters yielding an effective acceleration due to the grainy structure of the Dark Matter given by

$$\dot{\boldsymbol{v}}_{\mathbf{df}} = \int \boldsymbol{\Delta v}_{\mathbf{M}}\mathrm{d}\nu(b,V_0) - \dot{\boldsymbol{v}}_{\mathbf{M0}} \equiv \dot{\boldsymbol{v}}_{\mathbf{M}\|} + \dot{\boldsymbol{v}}_{\mathbf{M}\perp} \quad . \qquad (8)$$

Since the correction due to the unperturbed orbits is parallel to $\boldsymbol{b}$, it affects the perpendicular component only. We find from Eqs. 3 and 4

$$\dot{\boldsymbol{v}}_{\mathbf{M}\|} = \int\frac{2Gmn(\boldsymbol{r})f(\boldsymbol{v})}{a(V_0)}\frac{\boldsymbol{V_0}}{V_0}\left[1+\frac{b^2}{a(V_0)^2}\right]^{-1}\mathrm{d}p\mathrm{d}q\mathrm{d}^3V_0 \qquad (9)$$

$$\begin{aligned}\dot{\boldsymbol{v}}_{\mathbf{M}\perp} &= \int\left(\frac{2Gmn(\boldsymbol{r})f(\boldsymbol{v})\boldsymbol{b}}{a(V_0)^2}\left[1+\frac{b^2}{a(V_0)^2}\right]^{-1}\right. \\ &\qquad \left.-\frac{2Gmn(\boldsymbol{r})f(\boldsymbol{v})\boldsymbol{b}}{b^2}\right)\mathrm{d}p\mathrm{d}q\mathrm{d}^3V_0 \\ &= \int\frac{-2Gmn(\boldsymbol{r})f(\boldsymbol{v})\boldsymbol{b}}{b^2}\left[1+\frac{b^2}{a(V_0)^2}\right]^{-1}\mathrm{d}p\mathrm{d}q\mathrm{d}^3V_0 \qquad (10)\end{aligned}$$

For the integration over impact parameters we expand the local density distribution up to first order in the (p,q)-plane

$$n(r)\approx n_0+\boldsymbol{b}\cdot\boldsymbol{n}_\perp \quad \text{with} \quad \boldsymbol{r}=\boldsymbol{r}_{\mathbf{M}}+\boldsymbol{b} \quad . \qquad (11)$$

Here $n_0 = n(\boldsymbol{r})|_{\mathrm{r_M}}$ and for the local density gradient we use the abbreviations

$$\begin{aligned}\boldsymbol{n_r} &\equiv \nabla n(\boldsymbol{r})|_{\mathrm{r_M}} \equiv (n_x,n_y,n_z) \equiv (n_p,n_q,n_s) \quad \text{and} \qquad (12)\\ \boldsymbol{n}_\perp &= \boldsymbol{n_r}-(\boldsymbol{n_r}\cdot\boldsymbol{e}_{\mathbf{V_0}})\boldsymbol{e}_{\mathbf{V_0}} = (n_p,n_q) \qquad (13)\end{aligned}$$

with coordinate systems (x,y,z) oriented at the velocity of the satellite with z axis parallel to $\boldsymbol{v}_{\mathbf{M}}$, and (p,q,s) with s axis parallel to $\boldsymbol{V_0}$ (both are locally centred at $\boldsymbol{r}_{\mathbf{M}}$, see Fig. 12). The vector $\boldsymbol{n}_\perp$ is the component of the density gradient perpendicular to $\boldsymbol{V_0}$. In the Taylor expansion an additional variation of $f(\boldsymbol{v})$ is neglected. So, for example, we do not account for some spatial variation of the velocity dispersion $\sigma(r)$.

2.2. Symmetries and general properties

There are two important features of the velocity changes due to 2-body encounters, the symmetries and the mass dependence. Both are fundamentally different for the parallel and the perpendicular component.

$\boldsymbol{\Delta v}_{\mathbf{M}\|}$: In the limit of small angle deflections ($b \ll a(V_0)$) the parallel component is proportional to the mass $M+m$ leading to the well known mass segregation. This also allows easily a separation from mean field effects.

The parallel component is a function of b^2 only. Therefore in a local Taylor expansion of the distribution function only terms even in p and in q contribute to the integral over impact parameters. These are 0. order, 2. order (diagonal terms only), ...

The parallel component is odd in V_0. Therefore the contribution vanishes for vanishing satellite velocity v_{M}, if the distribution function $f(\boldsymbol{v})$ is symmetric.

$\boldsymbol{\Delta v}_{\mathbf{M}\perp}$: For small angles the perpendicular acceleration is proportional to $(M+m)^2$ leading to a stronger mass dependence. On the other hand, the acceleration falls off steeper with V_0 leading to a dominating contribution at small V_0.

The perpendicular component is odd in $\boldsymbol{b}$, though terms odd in p or q in the Taylor expansion of the distribution function contribute to the integral over impact parameters. That are the 1. order, 3. order, ...

The perpendicular component is even in V_0. This has the effect, that there is a net acceleration also for vanishing v_{M} leading to a kind of drift antiparallel to the density gradient due to the asymmetric gravitational wake. This corresponds to an effective reduction of the enclosed mass $\mathcal{M}(r_{\mathrm{M}})$ of the Dark Matter halo due to the perturbation, reducing the mean field force.

These symmetries are relative to the velocity $\boldsymbol{V_0}$ and not to the velocity $\boldsymbol{v}_{\mathbf{M}}$ of the satellite through the Dark Matter! The directions of the accelerations relative to v_{M} depend on the symmetries of the distribution function $f(\boldsymbol{v})$. The 0. order (parallel component), that is standard Chandrasekhar, is parallel to v_{M} for an isotropic distribution function only. The 1. order (the dominating term of the perpendicular component) is not perpendicular to v_{M} even for an isotropic distribution function. For vanishing v_{M} and isotropic velocity distribution function it is antiparallel to the density gradient.

2.3. Integration over impact parameters

Before integrating over the impact parameters we discuss the minimum and maximum impact parameter.

Minimum impact parameter b_0: For a point mass there is a natural effective lower cutoff at $b = a(V_0)$, the 90 degree deflection. Since $M \gg m$, even in the case of large angle deflection the velocity change $\Delta\boldsymbol{v}_{\mathbf{M}}$ is small and can be handled as a perturbation (i.e. validity of using superposition of 2-body encounters). But for extended bodies, there is an additional effective b_0 determined by the typical radius of the satellite. An orientation at the half-mass radius r_h is a good choice with a correction factor of order unity, because the deflection angle is dominated by the force near the minimum distance, determined by the enclosed mass. For a Plummer sphere the half-mass radius is given by $r_h = GM/(4.6\sigma_0^2) = 1.3 r_c$ with central velocity dispersion σ_0 and core radius r_c (a detailed calculation of White (1976) corresponds to $b_0 = 1.6 r_c$). For a King profile the half-mass radius is between 1/3 and 1/4.6 of GM/σ_0^2. So

$$b_0 = \frac{GM}{4\sigma_0^2} \approx r_h \tag{14}$$

(which corresponds to the half mass radius of a singular isothermal sphere with outer cutoff) is a good estimate of the minimum impact parameter.

Maximum impact parameter b_1**:** The allowed (and effective) range of impact parameters is bounded by the geometry and by the relevant time scales. The local approximation of the distribution function brakes down for distances larger than the local scale length l. Therefore the maximum impact parameter should be smaller than l,

$$b < l \equiv \rho/|\nabla\rho| = n_0/|\boldsymbol{n_r}| \quad . \tag{15}$$

By using this cutoff, we neglect more distant encounters and underestimate dynamical friction. On the other hand an upper limit for b_1 contributing to the inhomogeneous force is the distance to the density maximum, that is the distance to the centre of the Dark Matter halo r_{M}. For an isothermal sphere $l = r_{\mathrm{M}}/2$. We account for this uncertainty of a factor of about two by using a fitting factor Q_2 for the maximum impact parameter.

The straight line approximation and the local approximation require, that the encounter time $t_{\mathrm{coll}} = 2b/V_0$ is short compared to the local dynamical timescale t_{dyn}, which is essentially determined by the local crossing time of the satellite $t_{\mathrm{dyn}} = l/v_{\mathrm{M}}$

$$\frac{2b}{V_0} = t_{\mathrm{coll}} < t_{\mathrm{dyn}} = \frac{l}{v_{\mathrm{M}}} \quad . \tag{16}$$

using normalised velocities $X = v_{\mathrm{M}}/(\sqrt{2}\sigma)$ and $W = V_0/(\sqrt{2}\sigma)$. So the maximum impact parameter depends on V_0 and is given by

$$b_1 = Q_2 l\, min[1, \frac{V_0}{2v_{\mathrm{M}}}] \approx Q_2 l \sqrt{\frac{W^2}{4X^2+W^2}} \quad . \tag{17}$$

In order to guarantee formally $b_1 > b_0$ also for very small V_0 we will use the analytic approximation

$$b_1^2 = b_0^2 + Q_2^2 l^2 \frac{W^2}{4X^2+W^2} \tag{18}$$

Since again it is a priory not clear, whether the timescale restriction does not exclude an important contribution of long term encounters, we will compare also with computations using a maximum impact parameter given by

$$b_{\mathrm{max}}^2 = b_0^2 + Q_1^2 l^2 \tag{19}$$

neglecting the time scale argument.

2.4. Homogeneous and inhomogeneous dynamical friction

For clarity we split the dynamical friction $\dot{\boldsymbol{v}}_{\mathbf{df}}$ (Eq. 8) into the part occurring from the homogeneous density term and that from the local density gradient (inhomogeneous friction)

$$\dot{\boldsymbol{v}}_{\mathbf{df}} \equiv \dot{\boldsymbol{v}}_{\mathbf{hom}} + \dot{\boldsymbol{v}}_{\mathbf{inh}} \tag{20}$$

From the symmetries we know that after integrating over impact parameters, only the parallel component $\dot{\boldsymbol{v}}_{\mathbf{M}||}$ contributes to the homogeneous friction $\dot{\boldsymbol{v}}_{\mathbf{hom}}$, and the perpendicular component $\dot{\boldsymbol{v}}_{\mathbf{M}\perp}$ to the inhomogeneous friction $\dot{\boldsymbol{v}}_{\mathbf{inh}}$. For comparison we calculate the standard case (homogeneous part, parallel component) in the same way as the inhomogeneous term. Inserting into Eq. 9 the Taylor expansion of the density (Eq. 11) and integrating over impact parameters gives (the gradient term vanish by symmetry after integration over angle ϕ from $\mathrm{d}p\mathrm{d}q = \mathrm{d}\phi b \mathrm{d}b$)

$$\begin{aligned} \dot{\boldsymbol{v}}_{\mathbf{hom}} &= \int n_0 f(\boldsymbol{v}) \frac{2Gm\boldsymbol{V_0}}{a(V_0)V_0} \int_{b_0^2}^{b_1^2} \left[1 + \frac{b^2}{a(V_0)^2}\right]^{-1} \pi \mathrm{d}b^2 \mathrm{d}^3 V_0 \\ &= 4\pi G m n_0 \int \frac{\boldsymbol{V_0}}{V_0} a(V_0) \ln(\Lambda) f(\boldsymbol{v}) \mathrm{d}^3 V_0 \end{aligned} \tag{21}$$

$$\text{with} \quad \Lambda = \sqrt{\left(1 + \frac{b_1^2}{a(V_0)^2}\right) \Big/ \left(1 + \frac{b_0^2}{a(V_0)^2}\right)} \tag{22}$$

The inhomogeneous term arises from the leading contribution of the perpendicular acceleration and gives the dominant contribution to the acceleration perpendicular to $\boldsymbol{V_0}$. The integration over the angle ϕ leads to

$$\int_0^{2\pi} (\boldsymbol{b} \cdot \boldsymbol{n}_\perp) \boldsymbol{b} \mathrm{d}\phi = \pi b^2 \boldsymbol{n}_\perp \quad . \tag{23}$$

Using this for the integration of Eq. 10 over impact parameters we find

$$\begin{aligned} \dot{\boldsymbol{v}}_{\mathbf{inh}} &= -\int \pi G m \boldsymbol{n}_\perp f(\boldsymbol{v}) \int_{b_0^2}^{b_1^2} \left[1 + \frac{b^2}{a(V_0)^2}\right]^{-1} \mathrm{d}b^2 \mathrm{d}^3 V_0 \\ &= -2\pi G m \int \boldsymbol{n}_\perp a(V_0)^2 \ln(\Lambda) f(\boldsymbol{v}) \mathrm{d}^3 V_0 \end{aligned} \tag{24}$$

where the gradient term of the Taylor expansion of the density contributes only. Please note, that $\boldsymbol{n}_\perp$, the density gradient perpendicular to $\boldsymbol{V_0}$, is a function of $\boldsymbol{V_0}$ leading to a more complicated angle integral in velocity space.

2.5. The Coulomb logarithm

With Eqs. 5 and 14 we can reformulate the Coulomb logarithm using two scaling parameters instead of the dependence on b_0, b_1, and the mass M. With the size ratio q_{d} and the ratio of specific kinetic energies q_{s} defined by

$$q_{\mathrm{d}} = \frac{l}{b_0} \qquad q_{\mathrm{s}} = \frac{\sigma^2}{\sigma_0^2} \tag{25}$$

we can write

$$a(V_0) \approx \frac{GM}{V_0^2} = \frac{2b_0}{q_{\mathrm{s}} W^2} \tag{26}$$

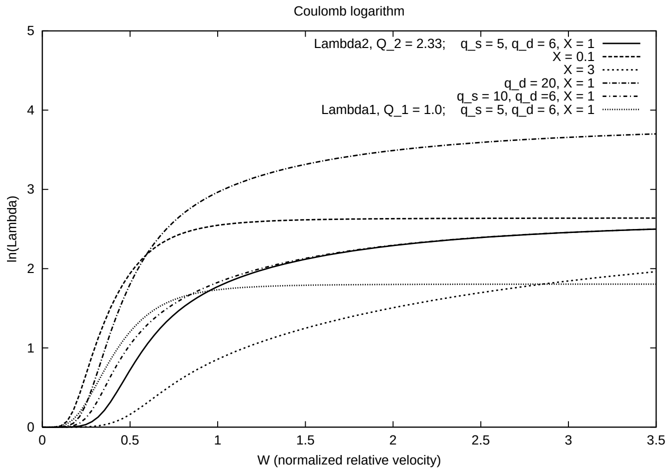

Fig. 1. The full line shows the Coulomb logarithm $\ln(\Lambda_2)$ with $Q_2 = 2.33$ (see Eq. 27) as a function of relative velocity $W = V_0/(\sqrt{2}\sigma)$ for a satellite with parameters $q_\mathrm{d}, q_\mathrm{s}$ and velocity $X = v_\mathrm{M}/(\sqrt{2}\sigma) = 1$ corresponding to a mass of $M = 5.6 \cdot 10^9 M_\odot$ moving on a circular orbit with radius $r_\mathrm{M} = 17$ kpc in the Dark Matter halo of the Milky Way. The variation with X (dashed lines), and for a more distant position (long dashed-dotted line) or a less massive satellite (short dashed-dotted line) are also plotted. For comparison the Coulomb logarithm $\ln(\Lambda_1)$ (see Eq. 28) is shown. We have chosen $Q_1 = 1.0$ in order to get the same homogeneous friction for $X = 1$.

Inserting this into Eq. 22 we get for the Coulomb logarithm with Eq. 18 the analytic approximation

$$\ln \Lambda_2 = \ln \sqrt{\frac{1 + \frac{W^4}{4} q_\mathrm{s}^2 \left(1 + Q_2^2 q_\mathrm{d}^2 \frac{W^2}{W^2+4X^2}\right)}{1 + \frac{W^4}{4} q_\mathrm{s}^2}} \tag{27}$$

and alternatively with Eq. 19

$$\ln \Lambda_1 = \ln \sqrt{\frac{1 + \frac{W^4}{4} q_\mathrm{s}^2 \left(1 + Q_1^2 q_\mathrm{d}^2\right)}{1 + \frac{W^4}{4} q_\mathrm{s}^2}} \quad . \tag{28}$$

For comparison with former results we will use also the simple approximations

$$\ln \Lambda_0 = \ln(Q_0 q_\mathrm{d}) \tag{29}$$

independent of relative velocity V_0, but dependent on position of the satellite, and also the globally constant value $\langle \ln \Lambda \rangle$.

In the case of an isothermal halo we can substitute q_d by using the mass ratio of the enclosed mass of the Dark Matter halo $\mathcal{M}(r_\mathrm{M})$ and the mass of the satellite with

$$l = \frac{r_\mathrm{M}}{2} \qquad \mathcal{M}(r_\mathrm{M}) = 4\pi m n(r_\mathrm{M}) r_\mathrm{M}^3 = \frac{2\sigma^2 r_\mathrm{M}}{G} \tag{30}$$

$$q_\mathrm{m} = \frac{\mathcal{M}(r_\mathrm{M})}{M} = q_\mathrm{s} q_\mathrm{d} \quad . \tag{31}$$

The Coulomb logarithm becomes

$$\ln \Lambda_2 = \ln \sqrt{\frac{1 + \frac{W^4}{4} \left(q_\mathrm{s}^2 + Q_2^2 q_\mathrm{m}^2 \frac{W^2}{W^2+4X^2}\right)}{1 + \frac{W^4}{4} q_\mathrm{s}^2}} \tag{32}$$

In Fig. 1 the velocity dependence of the Coulomb logarithm is shown for different satellite velocities X and typical parameters $q_\mathrm{d}, q_\mathrm{s}$. $X = 1$ corresponds to a circular orbit in an isothermal halo. We show the full velocity dependent Coulomb logarithm $\ln(\Lambda_2)$ with $X = 1$. We have chosen $Q_2 = 2.33$, which is the best fit value for the typical orbit discussed below. For the standard dynamical friction (homogeneous term) the corresponding values are $Q_1 = 1.0$ and $Q_0 = 0.8$ to get a to get the same force for $X = 1$. For smaller X the cutoff at low relative velocities W is steeper, for higher X it becomes flatter (long and short dashed lines, respectively). At larger distances (bigger q_d), the Coulomb logarithm is larger and the cutoff is shifted to smaller values of W. A less massive satellite (larger q_s) also leads to a cutoff at lower W. For comparison the Coulomb logarithm $\ln(\Lambda_1)$ (dashed line) with constant b_max shows a smoother cutoff ($\propto W^4$ instead of W^6), which occurs at a lower relative velocity. The effect of the low velocity cutoff is discussed in detail in Sect. 3.

3. Homogeneous and inhomogeneous dynamical friction

For the integration over velocity space we restrict ourselves to isotropic velocity distribution functions $f(v^2)$. Allowing for an anisotropy combined with the local density gradient would lead to very complicated angle integrations, which can hardly be performed analytically. All details of the integrations in spherical coordinates in $\mathrm{d}^3 V_0$-space are given in the Appendix. Here we discuss the results for a Gaussian

$$f(v^2) = \frac{1}{(\sqrt{2\pi}\sigma)^3} \exp(-\frac{v^2}{2\sigma^2}) \tag{33}$$

for the explicite integration, but the general results do not depend strongly on the special shape of $f(v^2)$ and can be done in the same way for different functions.

The homogeneous friction term $\dot{\boldsymbol{v}}_\mathbf{hom}$ is parallel to the satellite motion $\boldsymbol{v}_\mathbf{M}$, whereas the inhomogeneous friction lies in the $(\boldsymbol{v}_\mathbf{M}, \boldsymbol{n_r})$-plane. Therefore we decompose the inhomogeneous term into the parallel and orthogonal components with respect to $\boldsymbol{v}_\mathbf{M}$

$$\begin{aligned} \dot{\boldsymbol{v}}_\mathbf{inh} &\equiv \dot{\boldsymbol{v}}_\mathbf{par} + \dot{\boldsymbol{v}}_\mathbf{ort} \quad \text{with} \\ \dot{\boldsymbol{v}}_\mathbf{par} &= (\dot{\boldsymbol{v}}_\mathbf{inh} \cdot \boldsymbol{e}_\mathbf{v_M}) \boldsymbol{e}_\mathbf{v_M} \\ \dot{\boldsymbol{v}}_\mathbf{ort} &= \dot{\boldsymbol{v}}_\mathbf{inh} - \dot{\boldsymbol{v}}_\mathbf{par} \quad . \end{aligned} \tag{34}$$

For comparison reasons of the different contributions to the friction we use the normalised functions $G_\mathrm{hom}(X)$, $G_\mathrm{par}(X)$, and $G_\mathrm{ort}(X)$

$$G_\mathrm{hom}(X) = \frac{\sqrt{\pi}}{2} \int_0^\infty \ln(\Lambda) \exp(-W^2 - X^2) \times \left[\cosh(2WX) - \frac{\sinh(2WX)}{2WX}\right] \frac{\mathrm{d}W}{WX} \tag{35}$$

$$G_\mathrm{par}(X) = \frac{\sqrt{\pi}}{2 q_\mathrm{d} q_\mathrm{s}} \int_0^\infty \ln(\Lambda) \exp(-W^2 - X^2) \times \left[\cosh(2WX) - \frac{\sinh(2WX)}{2WX}\right] \frac{\mathrm{d}W}{X^2 W^4} \tag{36}$$

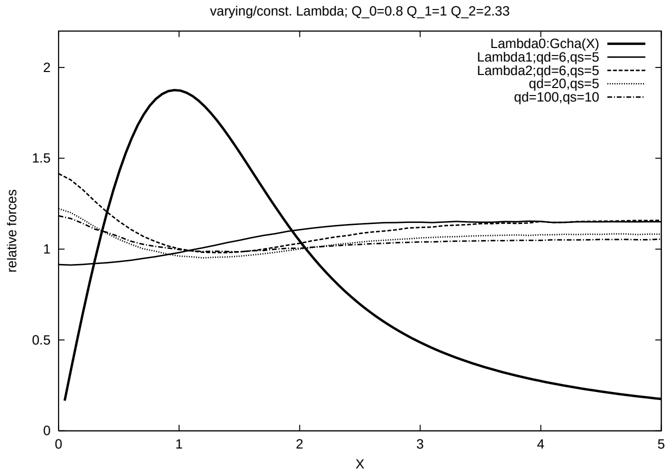

Fig. 2. The thick line shows the homogeneous force with velocity independent $\ln \Lambda_0$ using $Q_0 = 0.8$ and $q_\mathrm{d} = 6$. The effect of using the varying Coulomb logarithm $\ln \Lambda_2$ with $Q_2 = 2.33$ for different parameters $q_\mathrm{d}, q_\mathrm{s}$ are demonstrated by the ratios $G_\mathrm{hom}(\Lambda_2)/G_\mathrm{hom}(\Lambda_0)$. For comparison one case with $\ln \Lambda_1$ ($Q_1 = 1.0$) is also plotted.

$$G_\mathrm{ort}(X) = \frac{\sqrt{\pi}}{4 q_\mathrm{d} q_\mathrm{s}} \int_0^\infty \ln(\Lambda) \exp(-W^2 - X^2) \times \left[\sinh(2WX) \frac{4W^2X^2+1}{2WX} - \cosh(2WX)\right] \frac{\mathrm{d}W}{X^2W^4} \quad (37)$$

leading to

$$\dot{\boldsymbol{v}}_\mathbf{hom} = -C_\mathrm{Ch} G_\mathrm{hom}(X) \boldsymbol{e}_{\mathbf{v_M}} \quad (38)$$

$$\dot{\boldsymbol{v}}_\mathbf{par} = -C_\mathrm{Ch} G_\mathrm{par}(X) \cos(\Psi) \boldsymbol{e}_{\mathbf{v_M}} \quad (39)$$

$$\dot{\boldsymbol{v}}_\mathbf{ort} = -C_\mathrm{Ch} G_\mathrm{ort}(X) \sin(\Psi) \boldsymbol{e}_\mathbf{ort} \quad (40)$$

where the projection factors $\cos(\Psi)$ and $\sin(\Psi)$ of the density gradient with angle Ψ between $\boldsymbol{v}_\mathbf{M}$ and $\boldsymbol{n_r}$ (see Eq. 54) is accounted for explicitely. The scaling factor $1/(q_\mathrm{d} q_\mathrm{s})$ occurring in the inhomogeneous terms relative to the homogeneous term is included in the functions $G_\mathrm{par}(X)$, $G_\mathrm{ort}(X)$. The explicite derivation of these functions are given in the Appendix (see Eq. 69).

3.1. Homogeneous dynamical friction

It is well known that for the standard dynamical friction force the dependence of the Coulomb logarithm on the relative velocity W can be neglected. Here we confirm this result quantitatively to specify the parameter regime, where this approximation of using $\ln \Lambda_0$ holds. In Fig. 2 the relative deviations from the standard case are plotted as a function of satellite velocity X for different satellite parameters. The behaviour of using $\ln \Lambda_1$ or $\ln \Lambda_2$ is systematically different, but the deviations from the constant value exceed 10% for very low velocities only. This velocity regime is reached by the satellite in the outer parts of highly eccentric orbits only. Since the amount of circularisation of the orbit depends on the relative importance of the motion around apo- and peri-centre (see Sect. 5.1), it may be worthwhile to test varying Coulomb logarithms in that case.

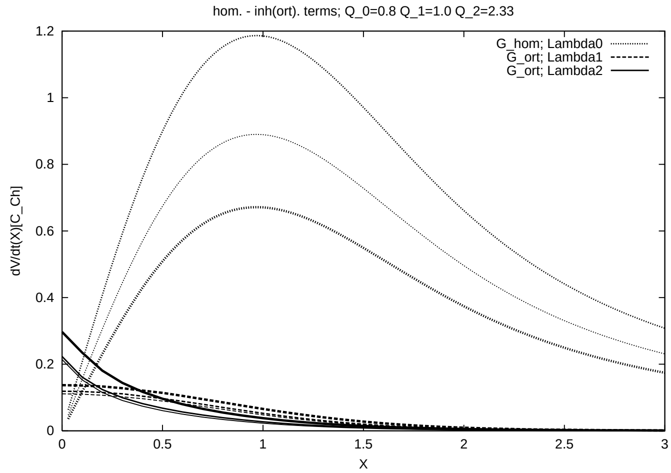

Fig. 3. The orthogonal component $G_\mathrm{ort}(X)$ of the inhomogeneous force is shown using the different Coulomb logarithms $\ln \Lambda_1$ ($Q_1 = 1.0$, dashed lines) and $\ln \Lambda_2$ ($Q_2 = 2.33$, full lines) compared to the homogeneous force with velocity independent $\ln \Lambda_0$ ($Q_0 = 1.0$, dotted lines). The functions for different parameters are plotted: $q_\mathrm{d} = 6$, $q_\mathrm{s} = 5$ thick lines; $q_\mathrm{d} = 20$, $q_\mathrm{s} = 5$ normal lines; $q_\mathrm{d} = 10$, $q_\mathrm{s} = 10$ thin lines.

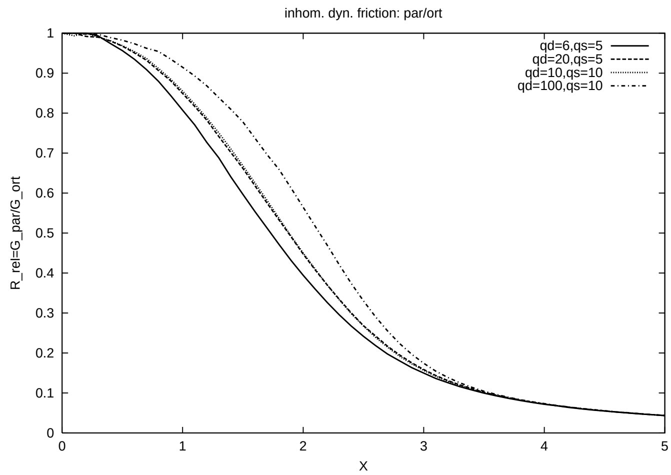

Fig. 4. The ratio of parallel and orthogonal contribution $G_\mathrm{par}(X)/G_\mathrm{ort}(X)$ to the inhomogeneous force for different parameters $q_\mathrm{d}, q_\mathrm{s}$.

In general, the velocity dependence of the Coulomb logarithm can be neglected. But the position dependence of $\ln \Lambda_0 = \ln(Q_0 q_\mathrm{d})$ is important (see Sect. 5).

3.2. Inhomogeneous dynamical friction

The properties of the inhomogeneous force given in Eqs. 39 and 40 are much more complicated. We first discuss $G_\mathrm{ort}(X)$, the component orthogonal to the satellite velocity. It gives the inhomogeneous force in units of C_Ch, if the density gradient is perpendicular to the satellite motion as in the peri- and apocentre. In Fig. 3 the contributions of G_ort using $\ln \Lambda_1$ and $\ln \Lambda_2$ are compared to G_hom with $\ln \Lambda_0$. We have chosen the corresponding best fit values $Q_0 = 0.8$, $Q_1 = 1.0$, and $Q_2 = 2.33$

for our standard orbit discussed in Sect. 5. With $\ln\Lambda_1$ the dependence of $G_{\rm ort}$ on X is relatively flat for low satellite velocities. In the most relevant regime between $0.5 < X < 2$ the force can exceed 15% of the homogeneous force. Using $\ln\Lambda_2$ leads to a steep decline with increasing satellite velocity X. For $X \approx 0$, the value is a factor of about 2 higher and for $X \approx 1$ it is a factor of 2 smaller. The magnitude is around a few and up to 10% of the homogeneous force. Along orbits with high eccentricity the inhomogeneous force can dominate over the homogeneous contribution around apo-centre. In this case there can a net acceleration before reaching apo-centre. The dynamics can be influenced significantly for these orbits due to a relative increase of the orbital time around apo-centre resulting in an enhancement of angular momentum loss. The figure also shows that the parameter dependence is quite different to the homogeneous force. The contribution from small impact parameters occurring in the dependence on the relative compactness parameter $q_{\rm s}$ plays a much larger role for the inhomogeneous force.

The component parallel to the satellite motion described by $G_{\rm par}$ is for $X > 0$ smaller than the orthogonal contribution (see Fig. 4). This results in a larger angle η of the inhomogeneous force $\dot{\boldsymbol{v}}_{\rm inh}$ with respect to $-\boldsymbol{v}_{\rm M}$ than the angle between the density gradient $\boldsymbol{n_r}$ and $\boldsymbol{v}_{\rm M}$. The inhomogeneous force is in the $(\boldsymbol{v}_{\rm M}, \boldsymbol{n_r})$ plane, and the angle η is given by

$$\tan(\eta) = \frac{\tan(\Psi)}{R_{\rm rel}(X)} \qquad \text{with} \qquad R_{\rm rel}(X) = \frac{G_{\rm par}(X)}{G_{\rm ort}(X)} \tag{41}$$

For small X the force is approximately parallel to $\boldsymbol{n_r}$, because $R_{\rm rel}(0) = 1$, and for large X the force is approximately parallel to $\boldsymbol{e}_{\rm ort}$ with $R_{\rm rel}(X) \propto X^{-2}$.

4. Satellite motion in Dark Matter haloes

In order to illustrate the effects that the different approximations for the Coulomb logarithm induce on the satellite motion in a DMH, we compare a N-body calculation with a semi analytical computation for a typical orbit. We use parameters representative of those observed for the Milky Way. A more detailed survey with numerical simulations will be presented in Peñarrubia et al. (2003). We have chosen a full simulations with a live satellite including mass loss during the decay in the live Milky Way DMH. With these comparisons we show the robustness of the improvements in the Coulomb logarithm and what can be expected from including the inhomogeneous friction term.

4.1. The galaxy and satellite parameters

Galaxy model: To avoid the strong effects of the disc on the satellite evolution, we employ a galaxy model formed purely by a DMH, with characteristics similar to those usually assumed for the Milky Way's halo. The density profile, therefore, can be approximated by a quasi-isothermal sphere with total mass M_h, core radius γ, and cut-off radius $r_{\rm cut}$ given by

$$\rho_h = \frac{M_h \alpha}{2\pi^{3/2} r_{\rm cut}} \frac{\exp(-r^2/r_{\rm cut}^2)}{r^2+\gamma^2}, \tag{42}$$

where the normalisation constant

$$\alpha \equiv \{1 - \sqrt{\pi}\beta\exp(\beta^2)[1-\mathrm{erf}(\beta)]\}^{-1} = 1 + \sqrt{\pi}\beta + (\pi-2)\beta^2 + O(\beta^3) \tag{43}$$

having $\beta = \gamma/r_{\rm cut}$. In our calculations we find with $\beta = 1/24$ $\alpha = 1.076 \simeq 1$. The initial distribution function in velocity space follows that of Eq. (33) with a cut-off at $v = v_e(r_{\rm M})$ the escape velocity of the system approximating dynamical equilibrium.

For normalisation of the physical units we set $G = 1$ and use the mass unit $M_d = 5.6 \times 10^{10} M_\odot$ and length unit $R_d = 3.5$kpc (typical disk values of the Milky Way, see Bahcall et al. (1982), which we adopt as a typical primary galaxy model). Then the time and velocity units are, respectively, 1.3×10^7 yr and $262\,\mathrm{kms}^{-1}$. With these units, the halo mass is $M_h = 14 M_d = 7.84 \times 10^{11}\mathrm{M}_\odot$ and $\gamma = R_d = 3.5$ kpc, whereas $r_{\rm cut} = 24 R_d = 84$ kpc. The number of halo particles is 1.4 10^6, all with equal mass.

Satellite model: We use a self-consistent King model (King 1966) to represent the satellite galaxy. These models fit early-type dwarf galaxies (Binggeli et al. 1984). For a comparison with the work of Peñarrubia, Kroupa & Boily (2001) we adopt $c = \log_{10}(r_t/r_c) = 0.8$ (corresponding to $\Phi_0/\sigma_0^2 = 5$), where $r_c = 1$ kpc and $r_t = 6.31$ kpc are the core and tidal radii, respectively. The satellite is formed by 40000 N-body particles, with a total mass of $M = 0.1 M_d = 5.60 \times 10^9\mathrm{M}_\odot$. The half-mass radius is $r_h = 1.33 r_c = 1.33$ kpc and the central velocity dispersion is $\sigma_0 = 52$ km/s.

Orbital parameters: We discuss the effects of dynamical friction using an eccentric orbit in the inner region of the DMH. We start the runs at apo-centre $r_0 = r_{\rm M}(t=0) = 55$ kpc with a tangential velocity $v(t=0) = \epsilon v_C$ with local circular velocity v_C from the rotation curve at the satellite's initial distance. We start with $\epsilon = 0.55$ leading to a first pericentre at $r_p \simeq 18$ kpc corresponding to an eccentricity of $e = (r_a - r_p)/(r_a + r_p) = 0.5$.

4.2. The N-body code

We use SUPERBOX (Fellhauer et al. 2000) to evolve the galaxy-satellite system. SUPERBOX is a highly efficient particle mesh-code based on a leap-frog scheme, and has been already implemented in an extensive study of satellite disruption by Peñarrubia et al. (2001) and Klessen & Kroupa (1998).

Our integration time step is 0.39 Myr which is about $1/25$th the dynamical time of the satellite. We have three resolution zones for the DMH, each with 64^3 grid-cells: (i) The inner grid covers 3 radial disc scale-lengths, providing a resolution of 350 pc per grid-cell. (ii) The middle grid covers the whole galaxy, with an extension of 24 disc scale-lengths (84 kpc) giving a resolution of 2.8 kpc per grid-cell. For most part of the evolution, the satellite is confined within this grid, which avoids cross-border effects (see Fellhauer et al. 2000). (iii) The outermost grid, which is common for all components, extends to 348 kpc and contains the local universe, at a resolution of 11.6 kpc.

As for the satellite grid-structure, the resolutions are 816 pc per grid-cell for the inner grid that extends to 24.48 kpc, 1.2 kpc per grid-cell for the middle grid which extends to 36 kpc. These satellite grids are moved together with the satellite.

4.3. The semi-analytical code

We have developed a simple numerical algorithm to integrate the equations of motion,

$$\ddot{\boldsymbol{r}}_{\boldsymbol{M}} = \nabla\Phi_g(r_{\rm M}) + \dot{\boldsymbol{v}}_{\bf df} \tag{44}$$

where Φ_g is the galaxy potential and $\dot{\boldsymbol{v}}_{\bf df}$ the dynamical friction acceleration acting on the satellite along the orbit. In this scheme, the DMH is represented by a rigid density profile $\rho_h(r)$ (Eq. 42), the local velocity dispersion is determined analytically from the Jeans equation. The satellite is represented by a point mass with assigned time-dependent mass $M(t)$ (taken from the mass loss in the N-body calculation) and a fixed half-mass radius $r_h = 1.33$ kpc. With these parameters the forces on the satellite are determined and the orbit can be calculated.

With this kind of semi analytical ansatz, the offset of the DMH to the centre-of-mass ($\simeq 1$ kpc) is neglected. Also the effect of mass loss on the specific momentum and energy of the satellite is not taken into account. After an evolution time of 2 Gyr, where mass loss exceed 10%, this seem to dominate over the influence of dynamical friction (see Sect. 5.1).

5. Results

In order to determine the accuracy of the analytical approaches and to fix the fitting parameter Q in the Coulomb logarithm, we propose a kind of mean square fit of the apo- and peri-centre values in space and time by minimising the parameter χ defined by

$$\chi^2 = \frac{1}{2k}\sum_{\rm i=1}^{2k}\left[(\boldsymbol{r_i} - \boldsymbol{r}_{\bf i,n})^2 + \sigma(r_0)^2(t_i - t_{\rm i,n})^2\right] \quad , \tag{45}$$

$\boldsymbol{r_i}$ being the position vectors at the peri- and apo-galacticons and t_i the time at which the satellite passes by these points in the semi analytical calculations. The subindex n denote the corresponding values of the N-body code and $\sigma(r_0)$ is the velocity dispersion at the initial galacto-centric distance. The sum is over a given number of orbits k. This definition of the fitting factor accounts for the deviation of the numerical and semi-analytical satellite position vectors and also the possibility that the curves of both orbit evolutions become out-of-phase in time. By definition, χ is equivalent to the discrepancy between the numerical and semi-analytical position evolution per unit orbit.

The resulting curves for χ are plotted in Fig. 5. The best fit to the numerical data occurs for $\langle\ln\Lambda\rangle = 2.1$ and $Q_2 = 2.33$ (the corresponding values are $Q_0 = 0.8$ and $Q_1 = 1.0$). The best fit value for Q is independent of the number of orbits taken into account, which likely indicates that the fit holds as a global fit. The distance evolution including the position dependent Λ_2 shows discrepancies to the numerical curve of the order of 25 per cent smaller than the global averaged Coulomb logarithm for the first three and four orbits. we find systematically smaller values for Q than Hashimoto et al (2002) give in their paper. They found a best fit value corresponding to $Q_0 = 2$ for the decay of a circular orbit using a point-mass satellite with a Plummer sphere potential. This is just the difference of using the distance to the DMH centre instead of the local sclae length.

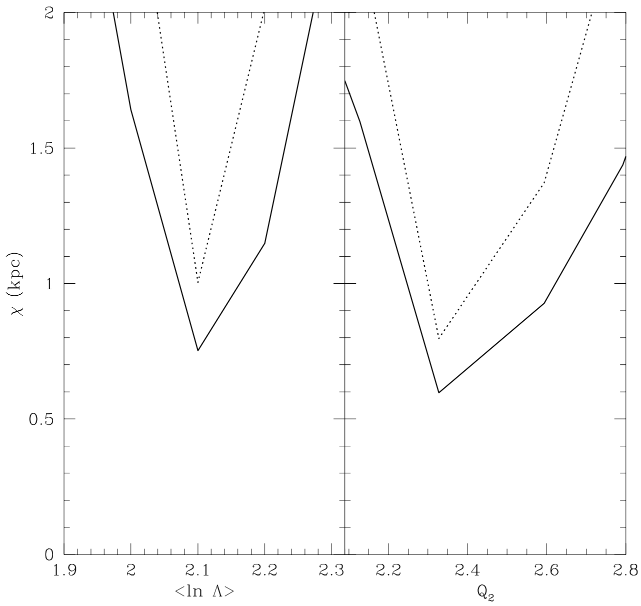

Fig. 5. Fitting factor χ as a function of the free parameters $\langle\ln\Lambda\rangle$ and Q_2. The measure of χ is done for two number of orbits, $k = 3, 4$ (solid and dotted lines respectively). We find a well defined minimum to determine the best fit values of $\langle\ln\Lambda\rangle = 2.1$ and $Q_2 = 2.33$.

In Fig. 6 we show the value of the Coulomb logarithm $\ln\Lambda_2$ along the satellite motion until reaching the first peri-centre using $W = X$ and the best fit value $Q_2 = 2.33$. The local maximum is due to the competing effects of decreasing scale length but increasing velocity dispersion. The constant value $\langle\ln\Lambda\rangle = 2.1$ and the radial run of the corresponding homogeneous friction forces are also plotted. The constant value $\langle\ln\Lambda\rangle$ equals the varying Coulomb logarithm at an inter-medium radius slightly shifted more to the peri-galacticon. Due to the density dependence of the dynamical friction, the forces are much stronger around peri-galaction. The relative variation along the orbit is reduced when using $\ln\Lambda_2$. The inhomogeneous force also shown in the figure is discussed in Sect. 5.2.

5.1. Orbit evolution

For a better understanding of the fitting results, we first analyse the effects that each analytical treatment of the Coulomb logarithm introduces to the orbital evolution of the satellite considering the dominant homogeneous friction force only.

In Fig. 7 the first 4 revolutions are shown in the orbital plane. There is a systematic delay in the precession rate of the N-body orbit compared to both semi-analytical approximations. The position dependent Coulomb logarithm gives a slightly better result. In Fig. 8 we compare the galacto-centre

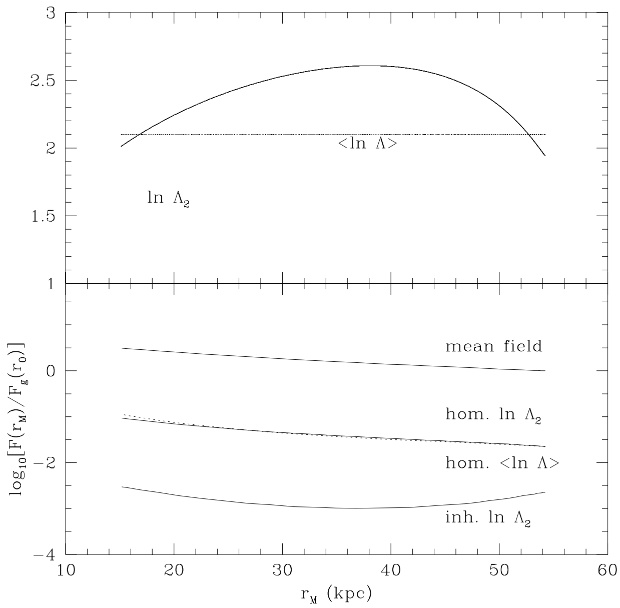

Fig. 6. Upper panel: Distance variation of $\ln \Lambda_2(X, W = X)$ with $Q_2 = 2.33$ (at $W = X$, where the dominant contribution to the friction arises) along the first orbit compared with the global averaged Coulomb logarithm $\langle \ln \Lambda \rangle = 2.1$. **Lower panel:** The mean field force $G\mathcal{M}(r_\mathrm{M})/r_\mathrm{M}^2$, the homogeneous friction forces $\dot{v}_\mathrm{hom}$ for both Coulomb logarithms and the inhomogeneous force $\dot{v}_\mathrm{inh}$ with $Q_2 = 2.33$ are plotted. All forces are normalised to the mean field force at apo-centre.

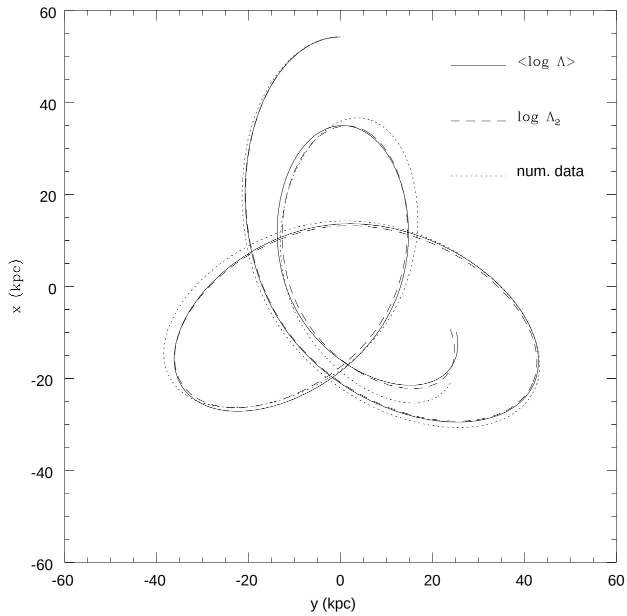

Fig. 7. Orbits in the analytical treatments including a global constant (solid line) and a distance dependent (dashed line) Coulomb logarithm compared to the numerical data (dotted line). The first 2.5 Gyr until reaching the fourth time apo-centre position is shown. orbits

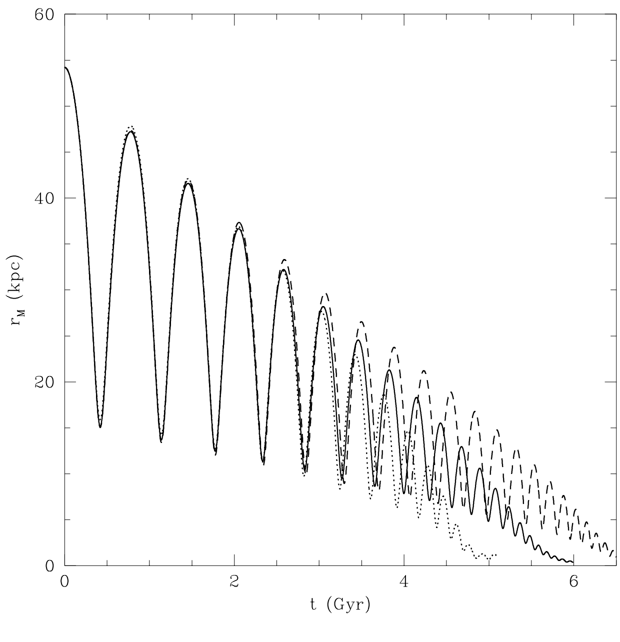

Fig. 8. Galacto-centre distance evolution of the same orbits as in Fig. 7 but over the whole lifetime of the satellite.

distance evolution of the analytic approaches to the Coulomb logarithm of Fig. 6. The addition of the radial dependence in the Coulomb logarithm reduces the friction at the peri-galacticon, so that the decay is less strong which, therefore, improves the fit to the numerical data.

This behaviour suffers a radical change at late times of the orbit. The numerical evolution of the galacto-centre distance shows a strong decrease of the apo- and peri-galacticon distances for $k > 7$, which can not be reproduced by any of the Coulomb factors that we employ. The approximation of constant Coulomb logarithm has more success, but this seems to be by chance only. The physical reason for this behaviour may be that the mass loss carries away additional momentum and energy, reducing the specific values for the remaining satellite. This is a matter of investigation in future work.

The evolution of specific energy E and angular momentum L due to drag forces show a different behaviour in eccentric orbits. With $\dot{E} = v_\mathrm{M}\dot{v}_\mathrm{df}$ and $\dot{L} = r_\mathrm{M}\dot{v}_\mathrm{df}\cos i = \frac{L}{v_\mathrm{M}}\dot{v}_\mathrm{df}$ (i is the inclination angle of the orbit relative to a circular motion) we can write the ratio of energy and angular momentum loss due to any drag force parallel to $\boldsymbol{v}_\mathrm{M}$ in the form

$$\frac{\dot{E}}{\dot{L}} = \frac{v_\mathrm{M}^2}{L} \tag{46}$$

which holds for all points along the orbit and is independent of eccentricity. The energy loss is strongly enhanced at the peri-centre, where the satellite velocity is larger. The result is shown in Fig. 9. The binding energy increases in steps at the peri-centres, whereas the angular momentum decreases quite smoothly. The evolution of the shape of the orbit, measured by the eccentricity e, depends on the values averaged over the whole revolution from apo- to apo-centre. If the energy loss dominates, the orbit will be circulised, and if angular momen-

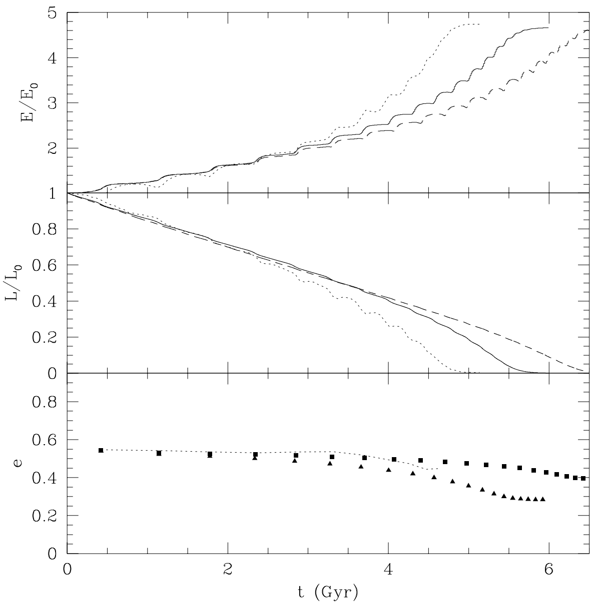

Fig. 9. Secular evolution of specific energy, angular momentum, and of the eccentricity e for the orbits as in Fig. 7. With constant Coulomb logarithm $\langle \ln \Lambda \rangle$ is the full curve, $\ln \Lambda_2$ the dashed line and the N-body simulation the dotted line. The values of e are given at pericentre (triangles for the constant Coulomb logarithm and squares for the varying Coulomb logarithm).

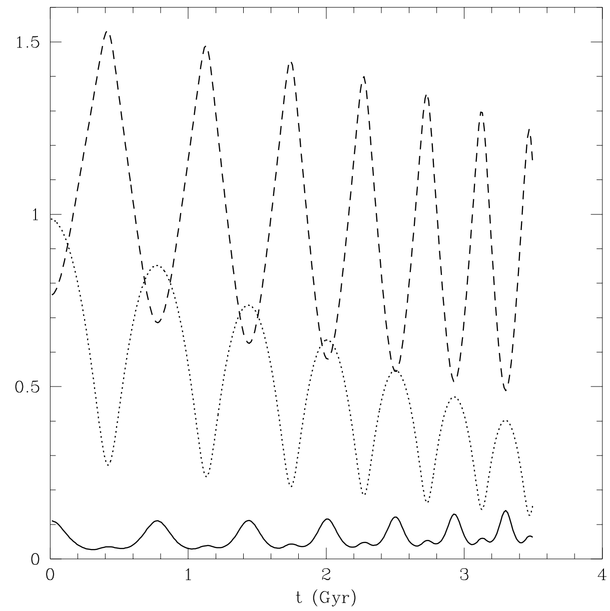

Fig. 10. Ratio of inhomogeneous to homogeneous force $\dot{v}_{\rm inh}/\dot{v}_{\rm hom}$ along the test orbit (full line). For a better understanding we also plot the radius $r_{\rm M}/r_0$ (dotted line) and satellite velocity $X(t)$ (dashed line).

tum loss dominates, the eccentricity will increase. The orbit with a constant Coulomb logarithm shows a significant circularisation, which is not observed in the N-body results (triangles compared to dotted line in the lower panel of Fig. 9). The varying Coulomb logarithm essentially solves this problem leading to constant shape of the orbit (squares in the figure). The enhanced energy and angular momentum loss of the N-body calculation at later times can be connected to the mass loss, whereas the local minima of the angular momentum curve at the peri-centres is artificial and due to the definition of bound particles by the tidal radius.

5.2. Inhomogeneous dynamical friction

Despite the problem of determining the maximum impact parameter, the inhomogeneity leads to the additional acceleration $\dot{\boldsymbol{v}}_{\rm \bf inh}$, which has, due to the different parameter dependence and direction relative to satellite motion (see Sect. 3), a different physical effect on the orbit.

In Fig. 10 we plot the ratio of the inhomogeneous and homogeneous force $\dot{\boldsymbol{v}}_{\rm \bf inh}/\dot{\boldsymbol{v}}_{\rm \bf hom}$ along the orbit. The maxima occur at the apo-galacticons. The small bump around the peri-galacticon shows the angle dependence of the inhomogeneous force being maximal, if the density gradient is perpendicular to the satellite motion. The magnitude of the forces are shown in Fig. 6. The mean value of the ratio slightly increases as the satellite sinks into the inner region of the galaxy. We conclude, therefore, that the inhomogeneous term is not negligible just by magnitude.

But if we compare the orbits with and without the inhomogeneous force (see Fig. 11), the correction is much smaller than expected form the forces, even around apo- and peri-centre. The main effects are a slight shift of the orbit to larger radii and a secular prolongation of the orbital time over large times.

For an understanding of this very small effect we can look on the decomposition of the inhomogeneous force into the parallel and orthogonal component (Eqs. 39 and 40). The parallel component can be considered as a correction to the homogeneous friction force, which changes sign when crossing the apo- and peri-galacticon. Therefore the main effect is a slight outside shift of the orbit. This can also be the reason for the slightly increasing orbital time of the satellite. There is no direct secular energy and momentum loss.

The orthogonal force leads to an additional bending of the orbits. It points outside and should reduce the curvature of the orbit like a reduction of the mean field. Since the force is nearly radial, the force adds to the mean field. This radial part works like a correction of the mean field by a few percent leading to a slightly different orbital shape with no secular part.

6. Discussion

We have recomputed the dynamical friction force on a massive body in a sea of lighter particles. We analysed in detail the properties and parameter dependences of the Coulomb logarithm $\ln \Lambda$, which is a measure of the 2-body encounters in the relevant range of impact parameters. We concentrated the investigation on the application to satellite galaxies in a dark

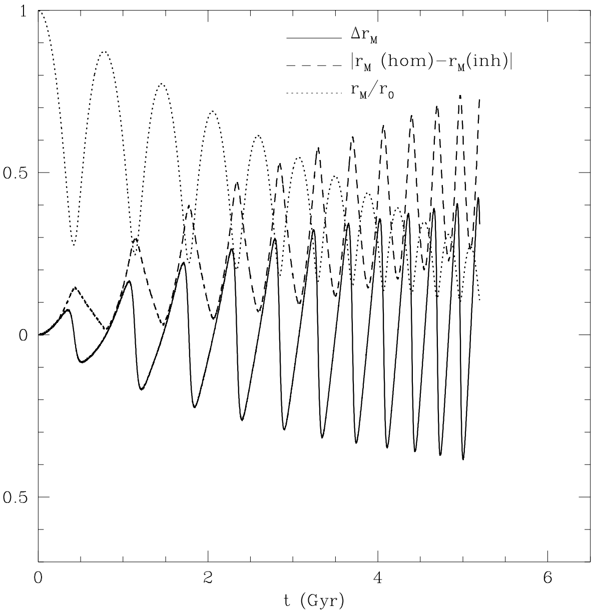

Fig. 11. Effects of the addition of the inhomogeneous friction term $\dot{\boldsymbol{v}}_{\mathbf{inh}}$ on the orbital evolution. Since the effects are small we show the radial distance difference of both orbits Δr_{M} (full line) and the difference in position $|\boldsymbol{r}_{\mathbf{M}}, hom - \boldsymbol{r}_{\mathbf{M}}, inh|$ (dashed line). For orientation the dotted line shows the position r_{M}/r_0 of the satellite.

matter halo (DMH) of the parent galaxy. Application to other systems are discussed below.

We have shown that the standard approximation of a velocity independent $\ln\Lambda$ is a good approximation (better than 10%) for most orbits and system parameters. In case of highly eccentric orbits corrections in the outer part of the orbit, where the satellite velocity is small, should be analysed. Especially for the question of circularisation it is important to use the correct relation of dynamical friction around peri-centre and apo-centre of the orbit (see below).

We investigated the effects of the inhomogeneity of the background distribution in two aspects. One is the determination of the maximum impact parameter leading to a position dependent $\ln\Lambda$ and the second one is the effect of the local density gradient on the friction force. The friction force due to the local (homogeneous) DMH density we call the 'homogeneous' term, which is in the simplest case the standard dynamical friction. The effect of the local density gradient leads to an additional 'inhomogeneous' term.

We first dicuss the homogeneous friction force. With the full parameter dependence of $\ln\Lambda$ (see Eq. 27) the maximum impact parameter is determined by the local density gradient (which is proportional to the distance to the DMH for power law profiles). This leads to a decreasing $\ln\Lambda$ with decreasing distance r_{M} of the satellite. The comparison of semi-analytical and N-body calculations show a significant improvement of the orbit fits especially for the precession rate in the orbital plane and the reduced circularisation. For the fitting factor Q, which allows to scale the effective cutoff of the impact parameter range, we find by comparison with N-body calculation using a live satellite and halo generally low values. This confirms the argument that the local scale length and not the distance to the halo centre determines effective range for impact parameters. This result shows a systematic difference to the recent results of Hashimoto at al. (2002). In order to distinguish between the local scale length or the distance to the DMH centre, it is necessary to investigate carefully different density profiles. Here especially the systematic effect of the variation in velocity dispersion is a crucial point. In this paper we neglected the effect of a velocity dispersion gradient.

If the satellite velocity is small enough around apo-centre, than the variation of the velocity dispersion along the orbit also changes $\ln\Lambda$. In our computations with a quasi-isothermal sphere with cutoff radius at 84 kpc, the variation of $\ln\Lambda$ due to the decreasing velocity dispersion with distance to the DMH centre competes with the increase due to the increasing scale length l.

The most important effect of a varying $\ln\Lambda$ is the reduction of the circularisation of the orbit. This seems to be a very sensitive quantity, because the effect is significant even in the case, where the dynamical friction force is changed by about 15% along the orbit only. The circularisation depends on the systematic parameter dependence of the friction force along the orbit, because the energy loss relative to angular momentum loss is strongly enhanced around peri-centre due to the higher satellite velocity (see Eq. 46). The general effect of a reduced friction force around peri-centre is a reduction of the energy loss leading to a lower circularisation.

For the calculation of the inhomogeneous force it is essential to use the velocity dependent $\ln\Lambda$ in order to have a robust and consistent cutoff at low impact velocities, where the dominant contribution arises (see Appendix for a comparison with Binney (1977), who used a lower cutoff velocity). The inhomogeneous force is for typical parameters about 10% relative to the homogeneous force. In highly eccentric orbits around apo-centre and for higher satellite masses ($\sim 10^{10} M_{\odot}$) it becomes significantly stronger. The force ratio of inhomogeneous and homogeneous terms scales essentially with $\sim M/\mathcal{M}(r_{\mathrm{M}})$ (the ratio of satellite mass and enclosed mass of the DMH). This is very similar to the ratio of the orbital to the friction time scale.

The properties of the inhomogeneous term is very different to the standard friction force. For an isotropic velocity distribution it is even in the satellite velocity leading to a non-vanishing force for $v_{\mathrm{M}} = 0$ and to a non-secular behaviour around apo- and peri-centre. The inhomogeneous force is more inclined to the satellite motion than the density gradient. For vanishing satellite motion it points anti-parallel to the density gradient. The parallel component gives an acceleration during outward motion and a deceleration during inward motion. The net force points outwards of the orbit leading to a less eccentric orbit. The inhomogeneous force mainly increases the duration of apo- and peri-centre crossing. This leads to a net increase of the orbital time and a reduction of the precession rate.

In our test orbit the effect of the inhomogeneous force is very small leading to an orbital offset of the order of 1 kpc over a few Gyr. But for increasing satellite mass or smaller peri-centre distances or smaller satellite velocity the inhomogeneous force is significantly higher relative to the standard dynamical friction force. In a further investigation we will discuss relevance of the inhomogeneous force in more detail.

The effect of the position dependent Coulomb logarithm on the circularisation of the orbits is in any case important for eccentric orbits. The general finding of constant or increasing eccentricity in N-body simulations can be may be understood in this way. The effect of the inhomogeneous force for other systems like the motion of super-massive Black holes in Galaxy centres can be estimated by checking the density gradient and the mass ratio of the object relative to the enclosed mass. Especially for highly eccentric orbits the inhomogeneous force can change the orbit evolution significantly.

The motion of SMBHs in the centres of cuspy dark matter haloes may also be affected significantly by corrections on the dynamical friction formula. The reason is teh relative high mass of the SMBH in the late phases of settling down at the centre and the numerically observed high eccentricities. In a following paper we will give a quantitative analysis of the motion of SMBHs in galactic centres.

References

Bahcall, J.N., Schmidt, M., Soneira, R.M. 1982, ApJ, 258, L23
Binggeli, B., Sandage, A., Tarenghi, M. 1984, AJ, 89, 64
Binney, J. 1977, MNRAS, 181, 735
Binney, J., Tremaine, S. 1987, Galactic Dynamics, Princeton Univ. Press, New Jersey
Chandrasekhar, S. 1943, ApJ, 97, 255
Fellhauer, M., Kroupa, P., Baumgardt, H., Bien, R., Boily, C.M., Spurzem, R., Wassmer, N. 2000, NewA, 5, 305
Hashimoto, Y., Funato, Y., Makino, J. 2002, ApJ, in press (astro-ph 0208452)
Just, A., Kegel, W.H., Deiss, B.M. 1986, A&A, 164, 337
Just, A., Kegel, W.H. 1990, A&A, 232, 447
King, I.R. 1966, AJ, 71, 65
Klessen, R.S., Kroupa, P. 1998, ApJ, 498, 143
Ostriker, E.C. 1999, ApJ, 513, 252
Peñarrubia, J., Just, A., Kroupa, P. 2003, in preparation
Peñarrubia, J., Kroupa, P., Boily, C.M. 2001, 333, 779, MNRAS
Peñarrubia, J. 2003, PhD Thesis, in preparation.
Del Popolo, A., Gambera, M. 1999, A&A, 342, 34
Sánches-Salcedo, F.J., Brandenburg, A. 1999, ApJ, 522, L35
Sánches-Salcedo, F.J., Brandenburg, A. 2001, MNRAS, 322, 67
Tremaine, S.D. 1976, ApJ, 203, 72
Tsuchiya, T., Shimada, M. 2000, ApJ, 532, 294
White, S.D.M. 1976, MNRAS, 174, 467

Appendix: Integration over velocity space

Coordinate systems

We discuss the simplest case of an isotropic velocity distribution function $f(v^2)$. Since the angle integration in $\boldsymbol{v}$-space is very complicated, for the inhomogeneous term at least, we use spherical coordinates in V_0-space oriented at v_M. This leads to

$$\mathrm{d}^3\boldsymbol{V_0} = -V_0^2 \mathrm{d}\varphi \mathrm{d}\mu \mathrm{d}V_0 \qquad \mu = \cos\theta \tag{47}$$

$$\boldsymbol{V_0} = V_0(\sqrt{1-\mu^2}\cos\varphi, \sqrt{1-\mu^2}\sin\varphi, \mu) \tag{48}$$

$$v^2 = |\boldsymbol{V_0} + \boldsymbol{v}_\mathbf{M}|^2 = V_0^2 + 2\mu V_0 v_\mathrm{M} + v_\mathrm{M}^2 \tag{49}$$

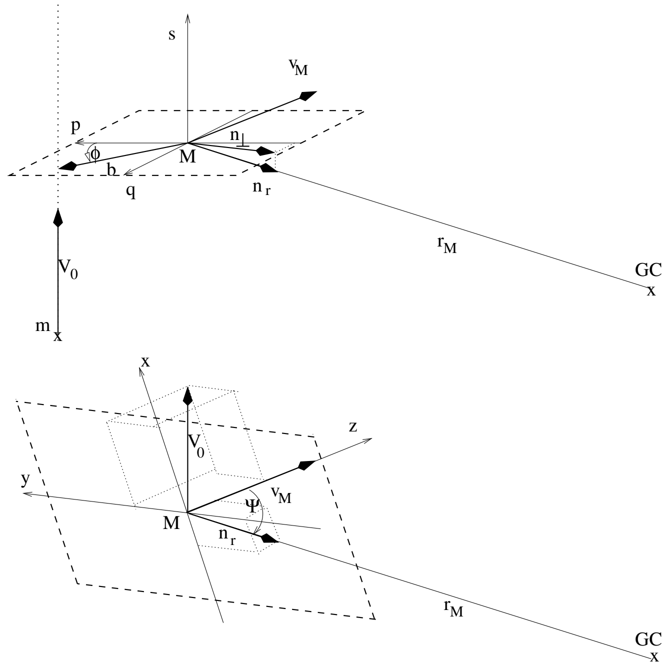

Fig. 12. Upper panel: Coordinate system centred at M (position $\boldsymbol{r}_\mathbf{M}$) oriented parallel to $\boldsymbol{V_0}$ for integration over impact parameter. **Lower panel:** Coordinate system centred at M oriented parallel to $\boldsymbol{v}_\mathbf{M}$ for integration over velocity space d^3V_0.

$$\begin{aligned}\boldsymbol{n}_\perp = \Big(& n_x - \cos\varphi\sqrt{1-\mu^2}[n_x\cos\varphi\sqrt{1-\mu^2} + \\ & \quad n_y \sin\varphi\sqrt{1-\mu^2} + n_z\mu], \\ & n_y - \sin\varphi\sqrt{1-\mu^2}[n_x\cos\varphi\sqrt{1-\mu^2} + \\ & \quad n_y \sin\varphi\sqrt{1-\mu^2} + n_z\mu], \\ & n_z - \mu[n_x\cos\varphi\sqrt{1-\mu^2} + \\ & \quad n_y \sin\varphi\sqrt{1-\mu^2} + n_z\mu]\Big)\end{aligned} \tag{50}$$

In the standard case the angle integrals are greatly simplified by using the general relation

$$h(V_0)\boldsymbol{e}_{\mathbf{V_0}} = \frac{\mathrm{d}}{\mathrm{d}\boldsymbol{V_0}}H(V_0) = -\frac{\mathrm{d}}{\mathrm{d}\boldsymbol{v}_\mathbf{M}}H(|v - v_\mathrm{M}|) \quad \text{with} \quad H'(V_0) = h(V_0) \tag{51}$$

and then integrating over v-space. But this method is not possible for the inhomogeneous term, because the dependence of $\boldsymbol{n}_\perp$ on $\boldsymbol{V_0}$ is more complicated. Therefore we integrate also for the homogeneous term directly over the angles.

Integration over φ

Since v^2 is independent of φ, we can integrate Eqs. 21 and 21 over φ without specifying the distribution function $f(v^2)$. We use

$$\int_0^{2\pi} \boldsymbol{e}_{\mathbf{V_0}} \mathrm{d}\varphi = 2\pi(0,0,\mu) = 2\pi\mu\boldsymbol{e}_{\mathbf{v_M}} \tag{52}$$

$$\int_0^{2\pi} \boldsymbol{n}_\perp \mathrm{d}\varphi = \pi\left([1+\mu^2]n_x, [1+\mu^2]n_y, 2[1-\mu^2]n_z\right)$$

$$= \pi \frac{n_0}{l} \left([1 + \mu^2] \sin \Psi \boldsymbol{e}_{\mathbf{ort}} + 2[1 - \mu^2] \cos \Psi \boldsymbol{e}_{\mathbf{v_M}} \right) \quad (53)$$

with $|\boldsymbol{n_r}| = n_0/l$ and using the decomposition of the density gradient with respect to $\boldsymbol{v}_\mathrm{M}$

$$\boldsymbol{n_r} = |\boldsymbol{n_r}| \left[\cos(\Psi) \boldsymbol{e}_{\mathbf{v_M}} + \sin(\Psi) \boldsymbol{e}_{\mathbf{ort}} \right] \quad (54)$$

where $\boldsymbol{e}_{\mathbf{ort}}$ is the unit vector in the direction of the orthogonal component of $\boldsymbol{n_r}$ and Ψ the angle between $\boldsymbol{v}_\mathrm{M}$ and $\boldsymbol{n_r}$. We split the inhomogeneous term in the same way into the parallel and orthogonal component (see Eq. 34). We find for the homogeneous acceleration term and the components of the inhomogeneous acceleration

$$\begin{aligned} \dot{\boldsymbol{v}}_{\mathbf{hom}} &= 4\pi G m n_0 \boldsymbol{e}_{\mathbf{v_M}} \times \\ &\int_0^\infty \int_{-1}^1 2\pi a(V_0) \ln(\Lambda) f(v^2) \mu \mathrm{d}\mu V_0^2 \mathrm{d}V_0 \quad (55) \\ \dot{\boldsymbol{v}}_{\mathbf{par}} &= \frac{-2\pi G m n_0}{l} \cos \Psi \boldsymbol{e}_{\mathbf{v_M}} \times \\ &\int_0^\infty \int_{-1}^1 2\pi a(V_0)^2 \ln(\Lambda) f(v^2)(1 - \mu^2) \mathrm{d}\mu V_0^2 \mathrm{d}V_0 \quad (56) \\ \dot{\boldsymbol{v}}_{\mathbf{ort}} &= \frac{-2\pi G m n_0}{l} \sin \Psi \boldsymbol{e}_{\mathbf{ort}} \times \\ &\int_0^\infty \int_{-1}^1 \pi a(V_0)^2 \ln(\Lambda) f(v^2)(1 + \mu^2) \mathrm{d}\mu V_0^2 \mathrm{d}V_0 \quad (57) \end{aligned}$$

The integral over μ

Since v^2 of the Dark Matter particles is a function of μ, we must specify the distribution function before going on. We use a Gaussian

$$\begin{aligned} f(v^2) &= \frac{1}{(\sqrt{2\pi}\sigma)^3} \exp(-\frac{v^2}{2\sigma^2}) \quad (58) \\ &= \frac{1}{(\sqrt{2\pi}\sigma)^3} \exp(-X^2 - W^2) \exp(-u\mu) \quad (59) \\ &\quad \text{with} \quad u = 2WX \end{aligned}$$

for the explicite integration, but the general results do not depend strongly on the special shape of $f(v^2)$. For the homogeneous term (Eq. 55) we need the integral

$$\begin{aligned} \int_{-1}^1 2\pi\mu \exp(-u\mu) \mathrm{d}\mu &= -4\pi \left[\frac{\cosh(u)}{u} - \frac{\sinh(u)}{u^2} \right] \quad (60) \\ &\approx \frac{-4\pi u}{3} \left(1 + \frac{u^2}{10} \right) \quad \text{for} \quad u \ll 1 \end{aligned}$$

and for the inhomogeneous components (Eqs. 56 and 57) the integrals

$$\begin{aligned} &\int_{-1}^1 \pi[1 + \mu^2] \exp(-u\mu) \mathrm{d}\mu = \\ &\quad -4\pi \left(\frac{\cosh(u)}{u^2} - \frac{1 + u^2}{u^3} \sinh(u) \right) \quad (61) \\ &\quad \approx \frac{8\pi}{3} \left(1 + \frac{u^2}{5} \right) \quad \text{for} \quad u \ll 1 \\ &\int_{-1}^1 2\pi[1 - \mu^2] \exp(-u\mu) \mathrm{d}\mu = \\ &\quad 8\pi \left(\frac{\cosh(u)}{u^2} - \frac{\sinh(u)}{u^3} \right) \quad (62) \\ &\quad \approx \frac{8\pi}{3} \left(1 + \frac{u^2}{10} \right) \quad \text{for} \quad u \ll 1 \end{aligned}$$

where for completeness the Taylor expansions for small velocities are also given.

Inserting the results of the angle integration into Eq. 56, we find for the homogeneous term

$$\begin{aligned} \dot{\boldsymbol{v}}_{\mathbf{hom}} &= -\frac{4\pi G^2 m(M + m) n_0}{\sqrt{\pi}\sigma^2} \frac{\boldsymbol{v}_\mathbf{M}}{v_\mathrm{M}} \int_0^\infty \ln\Lambda \times \\ &\exp(-W^2 - X^2) \left(\frac{\cosh(2WX)}{WX} - \frac{\sinh(2WX)}{2W^2X^2} \right) \mathrm{d}W \\ &= -C_\mathrm{Ch} \boldsymbol{e}_{\mathbf{v_M}} \int_0^\infty \ln(\Lambda) g_\mathrm{hom}(X, W) \mathrm{d}W \quad (63) \end{aligned}$$

Here we used C_Ch from Eq. 2 and the function

$$\begin{aligned} g_\mathrm{hom}(X, W) &= \frac{2}{\sqrt{\pi}} \exp(-W^2 - X^2) \left(\frac{\cosh(2WX)}{WX} - \right. \\ &\left. \frac{\sinh(2WX)}{2W^2X^2} \right) \quad (64) \end{aligned}$$

($\ln\Lambda$ is a function of V_0^2, too, see Eq. 22).

For the inhomogeneous terms we get from Eq. 56 the parallel component

$$\begin{aligned} \dot{\boldsymbol{v}}_{\mathbf{par}} &= \frac{-G^3 m(M + m)^2 \sqrt{\pi} n_r}{\sigma^4 X^2} \cos(\Psi) \boldsymbol{e}_{\mathbf{v_M}} \times \\ &\int_0^\infty \ln(\Lambda) \exp(-W^2 - X^2) \times \\ &\left(\cosh(2WX) - \frac{\sinh(2WX)}{2WX} \right) \frac{\mathrm{d}W}{W^4} \\ &= -C_\mathrm{Ch} \cos(\Psi) \boldsymbol{e}_{\mathbf{v_M}} \int_0^\infty \ln(\Lambda) g_\mathrm{par}(X, W) \mathrm{d}W \quad (65) \end{aligned}$$

and from Eq. 57 the orthogonal component

$$\begin{aligned} \dot{\boldsymbol{v}}_{\mathbf{ort}} &= \frac{-G^3 m(M + m)^2 \sqrt{\pi} n_r}{2\sigma^4 X^2} \sin(\Psi) \boldsymbol{e}_{\mathbf{ort}} \times \\ &\int_0^\infty \ln(\Lambda) \exp(-W^2 - X^2) \times \\ &\left(\frac{4W^2X^2 + 1}{2WX} \sinh(2WX) - \cosh(2WX) \right) \frac{\mathrm{d}W}{W^4} \\ &= -C_\mathrm{Ch} \sin(\Psi) \boldsymbol{e}_{\mathbf{ort}} \int_0^\infty \ln(\Lambda) g_\mathrm{ort}(X, W) \mathrm{d}W \quad (66) \end{aligned}$$

where we used analogous functions

$$\begin{aligned} g_\mathrm{par}(X, W) &= \frac{1}{q_\mathrm{d} q_\mathrm{s}} \frac{g_\mathrm{hom}(X, W)}{W^3 X} \quad (67) \\ g_\mathrm{ort}(X, W) &= \frac{1}{q_\mathrm{d} q_\mathrm{s}} \frac{2h(X, W) - g_\mathrm{hom}(X, W)}{2W^3 X} \quad \text{with} \quad (68) \\ h(X, W) &= \frac{2}{\sqrt{\pi}} \exp(-W^2 - X^2) \sinh(2WX) \end{aligned}$$

Now we can discuss the effect of the different approximations for the Coulomb logarithm (Eqs. 27, 28, 29). For the homogeneous force (arising from $\ln(\Lambda) g_\mathrm{hom}(X, W)$) the effect

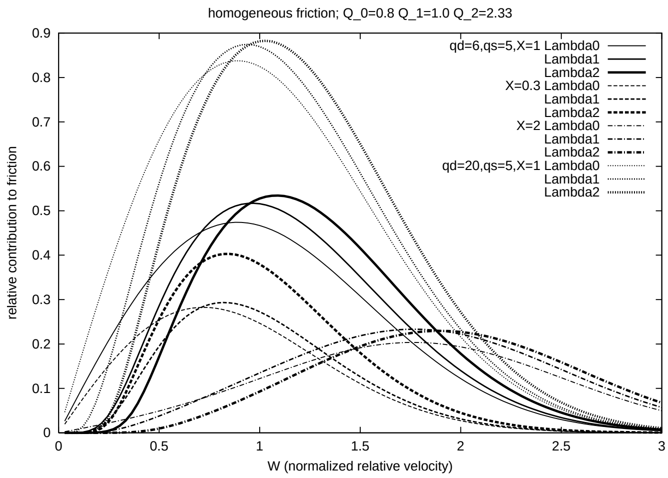

Fig. 13. Here we compare the contribution to the homogeneous dynamical friction as a function of encounter velocity W for different satellite velocities $X = 0.3, 1.0, 2.0$ using the different approximations for the Coulomb logarithm. We chose values $Q_0 = 0.8$ (corresponding to the standard dynamical friction; thin lines), $Q_1 = 1.0$ (normal lines), and $Q_2 = 2.33$ (thick lines) leading all to the similar homogeneous friction for $X = 1$. The system parameters are $q_{\rm d} = 6$ and $q_{\rm s} = 5$, but the systematic behaviour is similar for other values (see the comparison with a more distant satellite with $q_{\rm d} = 20$).

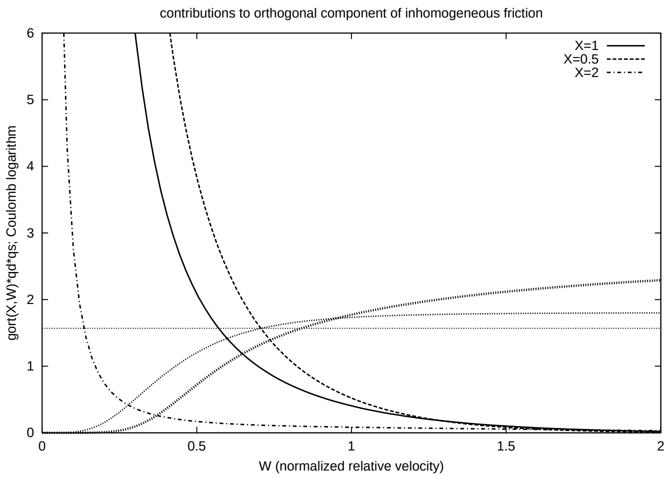

Fig. 14. Here the function $g_{\rm ort}(X, W) * (q_{\rm d} q_{\rm s})$ for the orthogonal component of the inhomogeneous dynamical friction as a function of encounter velocity W for different satellite velocities $X = 0.5, 1.0, 2.0$ is shown. It must be multiplied by the Coulomb logarithm, before integrating over W. The effect of using different approximations for the Coulomb logarithm is essential, because the dominating contribution comes from small W, where $g_{\rm ort}(X, W)$ has a strong singularity. For imagination the Coulomb logarithms with $q_{\rm d} = 6$, $q_{\rm s} = 5$, and $X = 1$ from Fig. 6 are plotted again (with $Q_0 = 0.8$, $Q_1 = 1.0$, $Q_2 = 2.33$ thin, normal, thick dotted line, respectively).

of the different Coulomb logarithms on the contributions as a function of W is shown in Fig. 13. The main effect of a varying Coulomb logarithm (with Q_1 or Q_2) is a shift of the dominant contribution to higher encounter velocities. But the overall deformation remains small and the dependence on the satellite motion is weak. Therefore one can use for the homogeneous friction force the approximation of a velocity independent Coulomb logarithm $\ln \Lambda_0$. The relative variation with X and dependence on the system parameters $q_{\rm d}, q_{\rm s}$ is shown in Fig. 2.

For the inhomogeneous force the effect of the Coulomb logarithm on both components ($g_{\rm par}(X, W)$ and $g_{\rm ort}(X, W)$) is similar. In Fig. 14 the parameter dependence of the Coulomb logarithm on the cutoff is demonstrated. The results on the contributions to the orthogonal component are shown in Fig. 15 using the same parameters as in Fig. 13. The main effect of a varying Coulomb logarithm (with Q_1 or Q_2) is a well defined lower cutoff consistent with the determination of $g_{\rm ort}(X, W)$ itself. The different approximations give significantly differing results. Therefore we will discuss both cases in detail. Using the approximation of a velocity independent Coulomb logarithm $\ln \Lambda_0$ can only be used together with a somewhat arbitrary cuttoff. This is not appropriate for applications due to the strong sensitiviy of the resultant force on the choice of the cutoff value (see below).

In Fig. 16 we show the contribution to the parallel force as a function of W relative to that for the orthogonal component. The parallel force is smaller for higher satellite velocities X, because the contribution from higher encounter velocities W is reduced with increasing X. Since the Coulomb logarithm determines mainly the contribution from small W, the effect on the orthogonal and the parallel components are similar .

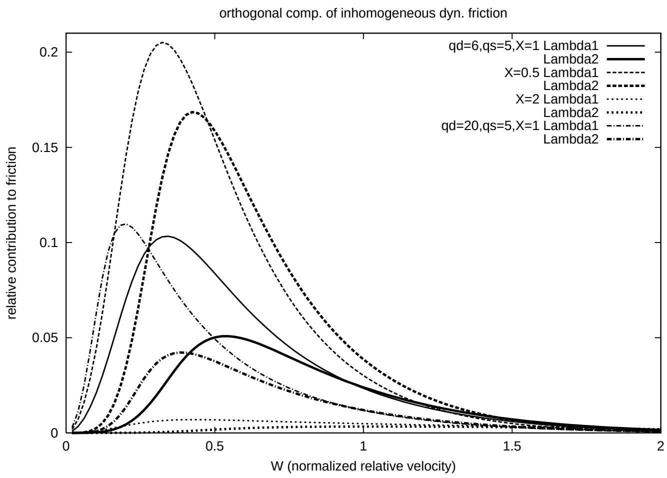

Fig. 15. Here the function $\ln(\Lambda) g_{\rm ort}(X, W)$ for the orthogonal component of the inhomogeneous dynamical friction as a function of encounter velocity W for different satellite velocities $X = 0.5, 1.0, 2.0$ is shown. The difference from using Λ_1 (thin lines) or Λ_2 (thick lines) is large and depends also on X and the system parameters $q_{\rm d}, q_{\rm s}$. The same values as in Fig. 13 are used.

Integration over V_0

We introduce now also the integrals of the normalized functions defined in Eqs. 64, 67, 68 by

$$G_{\rm cha,par,ort}(X) = \int_0^\infty \ln(\Lambda) g_{\rm cha,par,ort}(X, W) {\rm d}W \tag{69}$$

to get a convenient form for a discussion of the structure of the different contributions to dynamical friction (see Eqs. 38, 39,

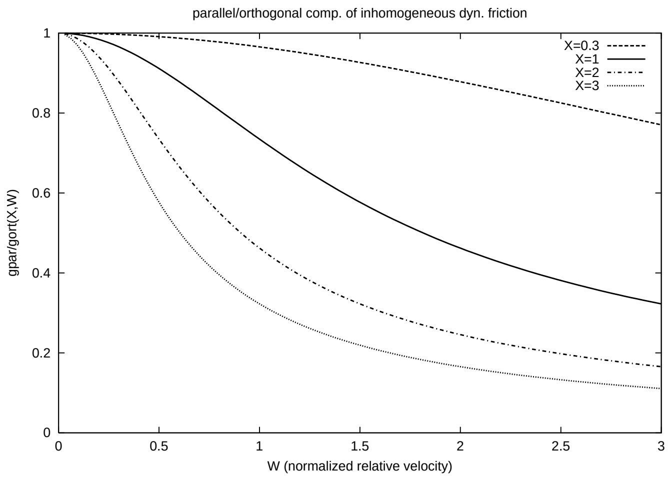

Fig. 16. Here the ratio $g_{\rm par}(X,W)/g_{\rm ort}(X,W)$ of the contributions to the parallel and orthogonal component of the inhomogeneous dynamical friction as a function of encounter velocity W for different satellite velocities $X=0.3, 1.0, 2.0, 3.0$ is shown.

40). With a velocity dependent Coulomb logarithm, the integration over W must be done numerically. Here we give the derivation of the standard friction formula and a short discussion of the behaviour of the inhomogeneous terms at low values of W. The explicite form of the integrals for the different contributions are given in Sect. 3 (Eqs. 35, 36, and 37). Further discussion of their properties is also given there.

Chandrasekhars friction formula

With the approximation of a Coulomb logarithm $\ln\Lambda_0$ independent of W (Eq. 29) we find the standard Chandrasekhar friction formula by integrating $g_{\rm hom}(X,W)$ (Eq. 64) by parts

$$\begin{aligned}\int_0^\infty g_{\rm hom}(X,W){\rm d}W &= \frac{2}{\sqrt{\pi}}\int_0^\infty \exp(-W^2-X^2)\times \\ &\quad\left(\frac{\cosh(2WX)}{WX}-\frac{\sinh(2WX)}{2W^2X^2}\right){\rm d}W \\ &= \frac{2}{\sqrt{\pi}X}\left[\exp(-W^2-X^2)\frac{\sinh(2WX)}{2WX}\Big|_0^\infty\right. \\ &\quad\left.+\frac{1}{X}\int_0^\infty \exp(-W^2-X^2)\sinh(2WX){\rm d}W\right] \\ &= \frac{2}{\sqrt{\pi}X}\left[-\exp(-X^2)+\frac{1}{2X}\int_{-{\rm X}}^{X}\exp(-Y^2){\rm d}Y\right] \\ &= \frac{1}{X^2}\left[erf(X)-\frac{2X}{\sqrt{\pi}}\exp(-X^2)\right]\end{aligned} \tag{70}$$

Inserting this into Eq. 63 we find the result

$$\dot{\boldsymbol{v}}_{\bf hom} \approx -C_{\rm Ch}\ln\Lambda_0\frac{\boldsymbol{e}_{\bf v_M}}{X^2}\left[erf(X)-\frac{2X}{\sqrt{\pi}}\exp(-X^2)\right] \tag{71}$$

Since the maximum impact parameter depends on the local scale length, the Coulomb logarithm depends on the position of the satellite. Neglecting this dependence also by using the global value $\langle\ln\Lambda\rangle$, we find the result given in Eq. 1.

Inhomogenous force and the lower cutoff

The functions $g_{\rm par}(X,W)$ and $g_{\rm ort}(X,W)$ show a singularity $\propto W^{-2}$ for vanishing W (Eqs. 67, 68). Since the velocity dependent Coulomb logarithms with Q_1 and Q_2 vansih for small W, i.e. $\ln\Lambda_1 \propto W^4$ and $\ln\Lambda_2 \propto W^6$, there is a natural effective lower cutoff for the integration over W. But the main contribution arises from low W just above this cutoff. This leads to differences of a factor of two at $X=0$, when using the corresponding best fit values $Q_1 = 1.0$ and $Q_2 = 2.33$ for the orbit.

If we want to use a velocity independent Coulomb logarithm $\ln\Lambda_0$, we must introduce a lower cutoff W_0. With a similar approximation as used by Binney (1977 Eq. (7)), we find for $X \ll 1$ the corresponding formula

$$\dot{v}_{\rm inh}(X) \approx C_{\rm Ch}\frac{8}{3\sqrt{\pi}}\frac{1}{q_{\rm d}q_{\rm s}}\frac{\langle\ln\Lambda\rangle}{W_0}\exp(-X^2) \tag{72}$$

Inserting the parameters at pericentre of our standard orbit $q_{\rm d}=6$, $q_{\rm s}=5$, $\langle\ln\Lambda\rangle=2.1$, and $G_{\rm ort}(X=0)=0.5$, we find the cutoff value $W_0=0.21$. We may compare this value with the relative velocity W_h for a 90-degree deflection at the half-mass radius r_h, which is

$$W_h = \sqrt{\frac{GM}{2\sigma^2 r_h}} = \sqrt{\frac{2}{q_{\rm s}}} = 0.63 \tag{73}$$

for the parameters above. Using W_h would give a factor of 3 to small friction force.